Card9 mediates susceptibility to intestinal pathogens through microbiota modulation and control of bacterial virulence

Bruno Lamas, Marie-Laure Michel, Nadine Waldschmitt, Hang-Phuong Pham, Vassiliki Zacharioudaki, Louise Dupraz, Myriam Delacre, Jane M Natividad, Gregory Da Costa, Julien Planchais, et al.

CARD9 MEDIATES SUSCEPTIBILITY TO INTESTINAL PATHOGENS THROUGH MICROBIOTA MODULATION AND CONTROL OF BACTERIAL VIRULENCE

Bruno Lamas[1,2], Marie-Laure Michel[2], Nadine Waldschmitt[3], Hang-Phuong Pham[4], Vassiliki Zacharioudaki[3], Louise Dupraz[2], Myriam Delacre[3], Jane M Natividad[2], Gregory Da Costa[2], Julien Planchais[2], Bruno Sovran[2], Chantal Bridonneau[2], Adrien Six[5], Philippe Langella[2], Mathias L. Richard[2], Mathias Chamaillard[3], Harry Sokol[6,7*].

[1]Sorbonne University – Université Pierre et Marie Curie (UPMC); Institut National de la Santé et de la Recherche Médicale (INSERM) Equipe de Recherche Labélisée (ERL) 1157, Avenir Team Gut Microbiota and Immunity; Centre National de Recherche Scientifique (CNRS) Unité Mixte de Recherche (UMR) 7203; Laboratoire de BioMolécules (LBM) Centre Hospitalo-Universitaire (CHU) Saint-Antoine 27 rue de Chaligny, Paris, France. [2]Micalis Institute, Institut National de la Recherche Agronomique (INRA), AgroParisTech, Université Paris-Saclay, 78350 Jouy en Josas, France. Inflammation-Immunopathology-Biotherapy Department (DHU i2B), Paris, France. [3]Institut Pasteur de Lille, Center for infection and immunity of Lille; INSERM U1019, Team 11, Equipe FRM, Lille, France. [4]ILTOO Pharma, 14 rue des Reculettes, Paris France. [5]Sorbonne Universités, UPMC Univ Paris 06, INSERM, UMRS959, Immunology-Immunopathology-Immunotherapy (I3), Paris, France. [6]Sorbonne University – UPMC; INSERM ERL 1157, Avenir Team Gut Microbiota and Immunity; CNRS UMR 7203; LBM CHU Saint-Antoine 27 rue de Chaligny; Micalis Institute, INRA, AgroParisTech, Université Paris-Saclay; DHU i2B, Paris, France. [7]Department of Gastroenterology, Saint Antoine Hospital, Assistance Publique – Hopitaux de Paris, UPMC, Paris, France.

[*]**Correspondence**: Pr Harry Sokol
Gastroenterology Department
Hôpital Saint-Antoine, 184 rue du Faubourg Saint-Antoine, 75571 Paris CEDEX 12, France
Tel.: +33 1 49 28 31 71
Fax: +33 1 49 28 31 88
E-mail: harry.sokol@aphp.fr

Word count: 3 970

Keywords: *Citrobacter rodentium*, mono- and polysaccharides, IBD, germfree mice, pathogen-specific antibody, microbiota

Abbreviations : CARD9: caspase recruitment domain 9; WT: wild-type; GF: germ-free; IBD: inflammatory bowel disease; EPEC: enteropathogenic *Escherichia coli*; EHEC: enterohemorrhagic *Escherichia coli*; PRR: pattern recognition receptor; AhR: aryl hydrocarbon receptor; PS: polysaccharides; MS: monosaccharides; LEE: locus for enterocyte effacement; ler: LEE-encoded-regulator; Lcn2: lipocalin 2; DSS: dextran sodium sulfate; MLN mesenteric lymph node; LDA: linear discriminant analysis; LEfSe: LDA effect size; SCFA: short chain fatty acid; ANOVA: one-way analysis of variance.

ABSTRACT

Objective In association with innate and adaptive immunity, the microbiota controls the colonization resistance against intestinal pathogens. Caspase recruitment domain 9 (*CARD9*), a key innate immunity gene, is required to shape a normal gut microbiota. *Card9*$^{-/-}$ mice are more susceptible to the enteric mouse pathogen *Citrobacter rodentium* that mimics human infections with enteropathogenic and enterohemorrhagic *Escherichia coli*. Here, we examined how *CARD9* controls *C. rodentium* infection susceptibility through microbiota-dependent and -independent mechanisms.

Design *C. rodentium* infection was assessed in conventional and germ-free (GF) wild-type (WT) and *Card9*$^{-/-}$ mice. To explore the impact of *Card9*$^{-/-}$ microbiota in infection susceptibility, GF WT mice were colonized with WT (WT→GF) or *Card9*$^{-/-}$ (*Card9*$^{-/-}$→GF) microbiota before *C. rodentium* infection. Microbiota composition was determined by 16S rDNA gene sequencing. Inflammation severity was determined by histology score and lipocalin level. Microbiota-host immune system interactions were assessed by qPCR analysis.

Results *CARD9* controls pathogen virulence in a microbiota-independent manner by supporting a specific humoral response. Higher susceptibility to *C. rodentium*-induced colitis was observed in *Card9*$^{-/-}$→GF mice. The microbiota of *Card9*$^{-/-}$ mice failed to outcompete the monosaccharide-consuming *C. rodentium,* worsening the infection severity. A polysaccharide-enriched diet counteracted the ecological advantage of *C. rodentium* and the defective pathogen-specific antibody response in *Card9*$^{-/-}$ mice.

Conclusions CARD9 modulates the susceptibility to intestinal infection by controlling the pathogen virulence in a microbiota-dependent and independent manner. Genetic susceptibility to intestinal pathogens can be overridden by diet intervention that restores humoral immunity and a competing microbiota.

Significance of this study

What is already known on this subject?

- In association with the genetic background, the gut microbiota participates in colonization resistance against pathogens directly by competing for food and indirectly by modulating the host immune response.
- CARD9, one of the inflammatory bowel disease (IBD) susceptibility gene, has a role in shaping the bacterial gut microbiota and is required for intestinal homeostasis.
- *Card9*$^{-/-}$ mice are more susceptible to the intestinal pathogen *Citrobacter rodentium* (that mimics human infections with enteropathogenic and enterohemorrhagic *Escherichia coli*) but the mechanisms are unknown.

What are the new findings?

- CARD9 promotes resistance to the enteric pathogens by gut microbiota dependent and independent mechanisms.
- CARD9 controls pathogen virulence in a microbiota-independent manner by supporting a specific humoral response.
- CARD9 participates also in colonization resistance against intestinal pathogens by shaping the gut microbiota which competes for sugars with pathogen.
- An appropriate diet intervention can override genetic susceptibility to intestinal pathogens by shaping the microbiota and promoting humoral immunity.

How might it impact on clinical practice in the foreseeable future?

- Our results demonstrate an interplay between diet, microbiota and IBD-predisposing genes which strongly influence colonization resistance against intestinal pathogens by supporting the immune response and shaping the gut microbiota.
- Dietary intervention supporting the host humoral response and depriving pathogens of food source or promoting bacteria that compete with pathogens for food source could be an interesting therapeutic strategy in patients with intestinal infection or with an intestinal disease involving Proteobacteria outgrowth, such as IBD.

INTRODUCTION

The gut microbiota is composed of highly diverse microbial communities that perform a wide variety of functions through direct or indirect interactions with the host. In humans, fecal microbiota transplantation is an effective therapeutic strategy to cure recurrent *Clostridium difficile* infections.[1] Thus, along with the genetic background, the gut microbiota can contribute to colonization resistance against pathogens directly by competing for food sources and indirectly by modulating the host immune response,[2 3] but the underlying host mechanisms have yet to be thoroughly described. These mechanisms can be explored using a murine colitis model induced by *Citrobacter rodentium*, a natural mouse pathogen widely used to mimic human infections with enteropathogenic *Escherichia coli* (EPEC) and enterohemorrhagic *E. coli* (EHEC),[4] which are important causes of diarrhea and mortality worldwide.[5 6] These gram-negative bacteria provoke transient enteritis or colitis by inducing attaching and effacing lesions on the intestinal epithelium.

Caspase recruitment domain family member 9 (*CARD9*) is an inflammatory bowel disease (IBD) susceptibility gene encoding an adaptor protein that integrates signals downstream of several pattern recognition receptors (PRRs).[7] In a previous study, we showed that *Card9*$^{-/-}$ mice are more susceptible to *C. rodentium* infection.[8] Moreover, we recently demonstrated that the bacterial and fungal microbiota of *Card9*$^{-/-}$ mice exhibit an impaired functional ability to catabolize tryptophan into aryl hydrocarbon receptor (AhR) ligands, leading to decreased IL-22 production by immune cells.[9]

The aim of the current study was to evaluate the microbiota-dependent and microbiota-independent roles of CARD9 in *C. rodentium* infection susceptibility. Here, we demonstrated that *Card9* is required for the *C. rodentium*-specific IgG response in a microbiota-independent manner and for shaping an intestinal microbiota able to compete with *C. rodentium* for nutrients. The microbiota of *Card9*$^{-/-}$ mice preferentially consumed polysaccharides and

failed to outcompete the monosaccharide-consuming *C. rodentium*. These mechanisms, associated with early defects in the IL-22 response, promoted a more severe infection, particularly in the early phase. This phenotype could be overridden by a diet containing polysaccharides (PSs) as the sole hydrocarbon source. The PS diet suppressed the ecological advantage of *C. rodentium* in the context of a low abundance of commensal competitors for monosaccharides (MSs) and counteracted the defective pathogen-specific antibody response observed in *Card9*$^{-/-}$ mice. These results showed that the interplay between diet and IBD-predisposing genes can strongly influence resistance to intestinal infections by modifying the immune response and the microbiota composition.

RESULTS

Intestinal pathogen-specific IgG response is altered in *Card9*$^{-/-}$ mice.

To evaluate the role of CARD9 in the response to *C. rodentium* infection, WT and *Card9*$^{-/-}$ mice were challenged with the *C. rodentium* strain DBS100 or a *C. rodentium* strain expressing luciferase. In accordance with previous work,[8] we observed higher susceptibility in *Card9*$^{-/-}$ mice compared to WT mice, with an increased *C. rodentium* fecal load (figure 1A) associated with a higher weight loss (figure 1B) and enhanced intestinal inflammation (figure 1C). Additionally, to evaluate the infection severity *in vivo*, we used a *C. rodentium* strain expressing luciferase and performed real-time whole body imaging. Four and 12 days after oral infection with *C. rodentium*, the bacterial load was higher in *Card9*$^{-/-}$ mice than in WT mice (see online supplementary figure S1A, B). We also observed increased levels of *C. rodentium* in the feces and cecum of *Card9*$^{-/-}$ mice at day 4 compared to WT mice (see online supplementary figure S1C-F). In a recent study, Kamada *et al.* showed that a specific antibody response targeting the Locus for Enterocyte Effacement (LEE) is required for selective elimination of virulent pathogens, while avirulent *C. rodentium* outcompeted by the

commensal microbiota were eradicated.[10] B cells from colon *lamina propria*, which are involved in intestinal Ig production were explored at baseline, but no differences were observed between WT and *Card9*$^{-/-}$ mice (see online supplementary figure S2). However, the specific intestinal IgG response against *C. rodentium* was impaired at day 12 post infection in *Card9*$^{-/-}$ mice compared to WT mice (figure 1D). This finding was associated with increased expression of the (LEE)-encoded-regulator (*ler)* gene in the feces of *Card9*$^{-/-}$ mice (figure 1E), which is a transcriptional activator of LEE virulence genes.[11] Overall, these data showed that the higher susceptibility of *Card9*$^{-/-}$ mice in the late phase of *C. rodentium* infection is at least partly mediated by defective intestinal humoral immunity and defective control of pathogen virulence.

Card9 controls pathogen virulence and the specific humoral response independently of the gut microbiota

To determine whether CARD9 controls *C. rodentium* infection in a gut microbiota-independent manner, germ-free (GF) WT and GF *Card9*$^{-/-}$ mice were challenged with *C. rodentium*. As previously reported,[12] GF WT mice cannot eradicate *C. rodentium,* and neither weight loss nor mortality was observed despite a high and persistent intestinal pathogen burden (figure 2A). The same results were observed in GF *Card9*$^{-/-}$ mice, with no difference in colonization between the two genetic backgrounds (figure 2A, see online supplementary figure S3). However, a significantly increased level of lipocalin 2 (Lcn2) and greater histopathological alterations indicated enhanced intestinal inflammation in GF *Card9*$^{-/-}$ mice compared to GF WT mice (figure 2B-D). Moreover, in GF *Card9*$^{-/-}$ mice, the specific intestinal IgG response against *C. rodentium* was impaired compared to GF WT mice (figure 2E). Accordingly, the expression of *ler* in *C. rodentium* was higher in the feces of GF *Card9*$^{-/-}$ mice compared to GF WT mice in the early and late phases of infection (figure 2F). *Rag2*$^{-/-}$

and *Rag2*$^{-/-}$*Card9*$^{-/-}$ mice exhibited a similar susceptibility to *C. rodentium*, supporting the idea that a defective humoral response is a key factor in the higher susceptibility of *Card9*$^{-/-}$ mice (see online supplementary figure S4). Collectively, these experiments showed that *Card9*$^{-/-}$ mice exhibit a defective intestinal humoral immunity response, leading to impaired elimination of virulent *C. rodentium* (*ler*+) and intestinal inflammation.

Card9$^{-/-}$ microbiota induces an IL22 defect at baseline but not during *C. rodentium* infection.

The gut microbiota is essential for the clearance of *C. rodentium* (figure 2A).[3 12] Moreover, we recently showed that the microbiota of *Card9*$^{-/-}$ mice contributes to the susceptibility of the mice to dextran sodium sulfate (DSS)-induced colitis by altering the IL-22 signaling pathway via impaired tryptophan metabolism, leading to defective AhR activation.[9] Therefore, we hypothesized that the higher susceptibility of *Card9*$^{-/-}$ mice to *C. rodentium* could also be related to the *Card9*$^{-/-}$ microbiota. To explore this hypothesis, we colonized GF WT mice with the microbiota of WT (WT→GF) or *Card9*$^{-/-}$ (*Card9*$^{-/-}$→GF) mice and challenged them with *C. rodentium* (see online supplementary figure S5). The cumulative bacterial loads (area under the curve) during the 3 weeks of infection were comparable in both groups (see online supplementary figure S6). However, *Card9*$^{-/-}$→GF mice were more susceptible than WT→GF mice to *C. rodentium,* with a higher fecal load of *C. rodentium* in *Card9*$^{-/-}$→GF mice in the early phase of infection until day 4 (figure 3A). A significantly increased level of Lcn2 and greater histopathological alterations indicated enhanced intestinal inflammation in infected *Card9*$^{-/-}$→GF mice (figure 3B-D). The strongest site of infection in both WT and *Card9*$^{-/-}$ mice was the cecum (see online supplementary figure S1D-F), as previously observed.[13] Therefore, to examine the mechanisms responsible for this defect, we compared the cecum transcriptomes of WT→GF and *Card9*$^{-/-}$→GF mice before and during

C. rodentium-induced colitis. The number of down-regulated and up-regulated genes on day 12 after infection was lower in *Card9*$^{-/-}$→GF mice than in WT→GF mice (see online supplementary figure S7). *Card9*$^{-/-}$→GF mice exhibited a significant down-regulation of genes involved in gut morphogenesis and wound healing pathways (see online supplementary figure S7A), suggesting that recovery is impaired in *Card9*$^{-/-}$→GF mice after *C. rodentium* infection. Immune response and cell division pathways were up-regulated in WT→GF mice but not in *Card9*$^{-/-}$→GF mice, confirming the presence of a defective global response to infection when only the *Card9*$^{-/-}$ microbiota was transferred (see online supplementary figure S7B). The most induced and differentially expressed genes between *Card9*$^{-/-}$→GF and WT→GF mice on day 4 after *C. rodentium* infection were the *Reg3γ* (encoding REGIIIγ) and *Reg3β* (encoding REGIIIβ) genes (figure 3E, see online supplementary figure S8). The IL-22 defect previously reported in the colons of *Card9*$^{-/-}$→GF mice[9] was confirmed by real-time quantitative PCR (qPCR) in the cecum and at the protein level in the mesenteric lymph nodes (MLNs) at baseline (figure 3F, G). This defect might play a role in the higher susceptibility of *Card9*$^{-/-}$→GF mice to *C. rodentium* infection, but it is probably minor, as IL-22 expression and production as well as *IL17A*, *Reg3β* and *Reg3γ* expression levels were normal or even higher than in WT→GF mice at day 4 and later during the infection. To determine whether the *Card9*$^{-/-}$ microbiota regulates LEE expression, we assessed the expression of *ler* in the feces of mice. A slight increase in the expression of *ler* was observed in *Card9*$^{-/-}$→GF mice at day 2 post-infection but not later during the infection (figure 3H). As expected, a comparable IgG response to the pathogen was observed between WT→GF and *Card9*$^{-/-}$→GF mice (see online supplementary figure S9). These results indicated that a defective IgG response in *Card9*$^{-/-}$→GF mice cannot explain their higher susceptibility to *C. rodentium* in the early phase of infection. Although other parameters might be involved, these results suggest a potential ecological effect.

***Card9*$^{-/-}$ microbiota exhibits decreased resilience upon *C. rodentium* infection.**

We next explored the composition of the microbiota at baseline and during the infection. A principal component analysis revealed major differences between the microbiota of WT→GF and *Card9*$^{-/-}$→GF mice throughout the experiment (figure 4A). The shift in microbiota composition during colitis followed a similar pattern in WT→GF and *Card9*$^{-/-}$→GF mice, but unlike WT→GF mice, the microbiota of *Card9*$^{-/-}$→GF mice did not return to its initial state at day 22 post infection (figure 4A-C). Alpha diversity measurements (Shannon index) also supported the observation of decreased resilience of the bacterial microbiota in *Card9*$^{-/-}$→GF mice (figure 4D). Indeed, no difference in alpha diversity was observed during the infection in WT→GF mice, whereas the diversity decreased between day 0 and day 22 in *Card9*$^{-/-}$→GF mice (figure 4D). Moreover, after pathogen clearance (day 22), the diversity was significantly lower in *Card9*$^{-/-}$→GF mice compared to WT→GF mice (figure 4D). Using the linear discriminant analysis (LDA) effect size (LEfSe) pipeline,[14] we observed several differences in the baseline fecal bacterial microbiota composition between *Card9*$^{-/-}$→GF mice and WT→GF mice, including increases in *Ruminococcus* genera in the *Card9*$^{-/-}$→GF mice (figure 4E, see online supplementary figure S10). To gain insight into the potential functional differences between the *Card9*$^{-/-}$→GF and WT→GF microbiota, we inferred metagenomes using the Picrust algorithm.[15] This analysis revealed several potential differences, most notably in hydrocarbon metabolism (see online supplementary figure S11). Indeed, functions related to monosaccharide (MS) use, such as fructose and mannose metabolism or galactose metabolism, were enriched in the WT→GF microbiota, whereas functions related to polysaccharide (PS) use, such as pyruvate and butanoate metabolism, were enriched in the *Card9*$^{-/-}$→GF microbiota (figure 4F, see online supplementary figure S11). Moreover, using 16S rDNA sequencing we recently demonstrated that the baseline bacterial microbiota of

Card9$^{-/-}$ mice was different than WT mice[9] and inferred metagenomes using the Picrust algorithm confirm that functions related to PS use could be enriched in *Card9*$^{-/-}$ microbiota (see online supplementary figure S12). Overall, these data demonstrate that the *Card9*$^{-/-}$ microbiota exhibits decreased resilience upon *C. rodentium* infection and suggest also that *Card9*$^{-/-}$ microbiota could have an imbalanced hydrocarbon metabolism favoring PS over MS.

Card9$^{-/-}$ microbiota fails to outcompete the monosaccharide-consuming _C. rodentium_.

As *C. rodentium* preferentially uses MSs,[12] we hypothesized that the higher susceptibility of *Card9*$^{-/-}$→GF mice could be related to the imbalance in the sugar metabolism of the gut microbiota toward PSs use, leading to a weaker competition for carbohydrate substrates with the pathogen. To test this hypothesis, WT and *Card9*$^{-/-}$ mice were fed a simple sugar diet containing either only MSs or only PSs as the sole hydrocarbon source and then challenged with *C. rodentium.* After 1 week of dietary intervention with either an MSs or PS diet, the gut microbiota composition was analyzed in WT and *Card9*$^{-/-}$ mice. Although the principal component analysis revealed microbiota differences between WT and *Card9*$^{-/-}$ mice, the diet effect seemed to dominate the host genotype in shaping the microbiota (figure 5A, see online supplementary figure S13). Interestingly, the diet effect was stronger in *Card9*$^{-/-}$ mice than in WT mice. Accordingly, no significant difference in alpha diversity (Shannon index) was observed between WT and *Card9*$^{-/-}$ mice regardless of the diet, whereas the diversity decreased in *Card9*$^{-/-}$ mice fed with PSs compared to *Card9*$^{-/-}$ mice fed with MSs (figure 5B). Using the LEfSe pipeline, we observed several diet-induced differences in the microbiota composition of WT and *Card9*$^{-/-}$ mice. Here again, the diet effect was stronger in *Card9*$^{-/-}$ mice, with a higher number of taxa differentially represented between mice fed an MS diet and those fed a PS diet, than in WT mice. One common diet-induced effect was that the PS

diet decreased the amount of Proteobacteria in both WT and *Card9*$^{-/-}$ mice (figure 5C). These results showed that favoring PSs intake over MSs has a detrimental effect on the intestinal colonization by Proteobacteria and suggested a potential positive effect in the context of infection with a Proteobacteria member such as *C. rodentium*. The MS diet increased the severity of *C. rodentium* infection in *Card9*$^{-/-}$ mice, with higher *C. rodentium* fecal load and weight loss, whereas the PS diet reversed the genetic susceptibility, resulting in a similar infection severity in *Card9*$^{-/-}$ and WT mice (figure 6A). Correspondingly, an increased level of Lcn2 and greater histopathological alterations indicated enhanced inflammation in *Card9*$^{-/-}$ mice fed the MS diet. In contrast, the PS diet decreased the infection severity in both WT and *Card9*$^{-/-}$ mice (figure 6B-D). As short chain fatty acids (SCFAs) are major microbial metabolites of polysaccharides[16 17] and support *C. rodentium*-specific antibody responses,[18] we hypothesized that the beneficial effect of the PS diet on the susceptibility of *Card9*$^{-/-}$ mice to *C. rodentium* (figure 4A) could be partly related to the increased production of intestinal IgG. We showed that the specific intestinal IgG response against *C. rodentium* was increased at day 12 in *Card9*$^{-/-}$ mice fed the PS diet compared to *Card9*$^{-/-}$ mice fed the MS diet (figure 6E). Interestingly, the specific intestinal humoral response was also defective at day 12 in WT mice fed the MS diet compared to WT mice fed the PS diet (figure 6E), suggesting that PSs are necessary for the basal production of *C. rodentium*-specific intestinal Igs. Consequently, the *ler* expression in feces was higher in *Card9*$^{-/-}$ mice fed MSs compared to *Card9*$^{-/-}$ and WT mice fed PSs at days 2 and 10 (figure 6F). Overall, these results show that *Card9* deletion shapes the microbiota, inducing a preferential use of PSs and leading to a lower competition for nutrients with *C. rodentium*. Moreover, a diet with PSs as the sole hydrocarbon source can override the genetic susceptibility of *Card9*$^{-/-}$ mice to intestinal pathogens by promoting a *C. rodentium*-specific antibody response, which leads to the elimination of virulent *C. rodentium*.

DISCUSSION

The gut microbiota is a key player in mammalian physiology and participates in the protection against intestinal pathogens. Several mechanisms are involved in this protection, including induction of host immune responses and competition for ecological niches and nutrients.[2 3] For instance, the transfer of the C57BL/6 microbiota is sufficient to overcome the inherent genetic susceptibility of C3H/HeOuJ mice to *C. rodentium* infection.[19] Here, we showed that *Card9* plays a key role in the response to *C. rodentium* infection through mechanisms that are both gut microbiota dependent and independent (figure 7). Using germ-free mice and microbiota transplantation experiments, we demonstrated that the interplay between diet and *Card9* expression regulates the virulence of *C. rodentium* to promote pathogen eradication and host survival.

C. rodentium-specific IgG antibodies are essential for pathogen clearance and host survival.[10 20 21] In the current study, we observed an impaired *C. rodentium*-specific IgG response in GF *Card9*$^{-/-}$ and *Card9*$^{-/-}$ mice during *C. rodentium* infection, suggesting that *Card9* controls the virulence of *C. rodentium* by supporting the specific humoral response independent of the gut microbiota.

GF animals are unable to eradicate pathogens, and the gut microbiota is essential for the clearance of *C. rodentium.*[3 12] Moreover, our previously published results demonstrated that the microbiota of *Card9*$^{-/-}$ mice is altered, with an impaired ability to catabolize tryptophan into AhR ligands, leading to decreased IL-22 production.[9] Here, we showed that transfer of the microbiota from *Card9*$^{-/-}$ mice to WT GF recipients was sufficient to recapitulate the increased susceptibility to *C. rodentium* observed in *Card9*$^{-/-}$ mice. IL-22 regulates mucosal wound healing,[22] is implicated in intestinal homeostasis,[23] triggers the secretion of antimicrobial proteins REGIIIγ and REGIIIβ by the intestinal epithelium[24 25] and is required

for protection against *C. rodentium* infection.[26 27] In the current study, we confirmed the baseline IL-22 defect in *Card9*$^{-/-}$→GF mice and, conversely, observed that the *Il22*, *Reg3b* and *Reg3g* expression levels were normal or higher compared to WT→GF mice during the infection. These two observations suggested that the baseline IL-22 defect contributes only marginally to the higher susceptibility of *Card9*$^{-/-}$→GF mice to *C. rodentium*.

Of equal importance, we noted an important ecological effect in the susceptibility of *Card9*$^{-/-}$ mice to *C. rodentium*. Indeed, several studies have shown that transfer of the microbiota of resistant mice to susceptible mice results in the transfer of host resistance to *C. rodentium* infection.[19 28 29] Resistance to *C. rodentium* infection has been previously associated with a decrease in Firmicutes and Porphyromonadaceae[28] and an increase in Bacteroidetes, Lachnospiraceae, Bacteroidaceae and an unclassified family of Clostridiales.[19 28] We observed increased levels of Firmicutes and decreased levels of the Clostridiaceae family in the baseline fecal bacterial microbiota composition in susceptible *Card9*$^{-/-}$→GF mice compared to resistant WT→GF mice. As these data were generated in different mice strains, they suggest a common ecological effect in the resistance to intestinal pathogens.

We further analyzed the microbiota metabolism and observed that the *Card9*$^{-/-}$ microbiota exhibits a deregulated hydrocarbon metabolism, favoring PSs over MSs, which leads to a lower competition for MSs and thus favors *C. rodentium* colonization. Previous studies have shown that *E. coli* competes with *C. rodentium* for available MSs and helps the host to clear the pathogen.[12] In accordance, the MS diet increased the severity of *C. rodentium* infection in *Card9*$^{-/-}$ mice, whereas the PS diet rescued the phenotype, showing that the PS diet can override the susceptibility of *Card9*$^{-/-}$ mice to *C. rodentium*. The PS diet induced a decrease in Proteobacteria in WT and *Card9*$^{-/-}$ mice, suggesting that dietary intervention can help protecting against intestinal infections in a genotype-independent manner by shaping the microbiota. *C. rodentium* is a Proteobacteria, which preferentially use MSs as a hydrocarbon

source,[12] suggesting that the PS diet was also involved in resistance to infection by decreasing the MSs availability for Proteobacteria such as *C. rodentium*. Moreover, SCFAs produced by the gut microbiota as fermentation products of PSs support the host antibody response.[18] In accordance, the PS diet promoted the *C. rodentium*-specific antibody response, which led to the elimination of virulent *C. rodentium* in *Card9*$^{-/-}$ mice, showing that the PS diet also contributed to the elimination of the pathogen by promoting humoral immunity.

Collectively, our study demonstrates that the IBD-predisposing gene *CARD9* plays a key role in controlling pathogen virulence and in shaping a balanced gut microbiota to eradicate luminal pathogens. Moreover, an appropriate diet can override genetic susceptibility to intestinal pathogens by shaping the microbiota and promoting humoral immunity. Indeed, dietary intervention supporting the host antibody response and depriving pathogens of a food source or promoting bacteria that compete with pathogens for the food source could be an interesting preventive or curative strategy in patients with intestinal infection or with an intestinal disease involving Proteobacteria outgrowth, such as IBD.[15]

MATERIALS AND METHODS

Animals

Card9-deficient mice (*Card9*$^{-/-}$)[30] and *Rag2*-deficient mice (*Rag2*$^{-/-}$), both in the C57BL/6J background, were crossed to generate *Rag2*$^{-/-}$/*Card9*$^{-/-}$ mice. All animals were housed under specific pathogen-free conditions at the Saint-Antoine Research Center. At weaning, the mice were separated according to genotype. Germ-free *Card9*$^{-/-}$ and C57BL/6J mice were bred in germ-free isolators at the CDTA (Transgénèse et Archivage d'Animaux Modèles, CNRS, UPS44, Orléans, France). Conventional mice were fed a standard chow diet (R03, SAFE), and germ-free mice were fed a diet without yeast (R04, SAFE). All conventional WT, *Card9*$^{-/-}$, *Rag2*$^{-/-}$ and *Rag2*$^{-/-}$*Card9*$^{-/-}$ mice used in this study were 8 weeks old. The animal

experiments were performed according to the institutional guidelines approved by the local ethics committee of the French authorities.

Gut microbiota transfer

Fresh stool samples preparation and gut microbiota transfer were performed as previously described [9] (see online supplementary data).

***Citrobacter rodentium* infection**

The *Citrobacter rodentium* strain DBS100 (ATCC 51459; American Type Culture Collection) was used for all inoculations with the exception of the bioluminescence experiments. The nalidixic acid-resistant and bioluminescent *C. rodentium* strain ICC180 was a gift from Dr. Casey T. Weaver (Department of Pathology, University of Alabama at Birmingham) and was used for the bioluminescence imaging experiments. The bacteria were grown overnight at 37°C in Luria broth supplemented or not with nalidixic acid (50 µg/ml) as appropriate. The mice were inoculated with *C. rodentium* as previously described.[8] The mice were infected by oral gavage with 0.5 ml of phosphate-buffered saline (PBS) containing approximately $1x10^9$ CFU of *C. rodentium*. To assess the clearance of *C. rodentium*, fecal pellets were collected from individual mice, homogenized in PBS, serially diluted, and plated onto selective MacConkey agar. After an overnight incubation at 37°C, colonies were counted based on the size and distinctive appearance of *C. rodentium* colonies as described previously.[8]

Custom rodent diet experiment

WT and *Card9*$^{-/-}$ mice were fed either a standard diet (TD. 120455, Envigo) or a customized version of Envigo TD. 120455 in which the polysaccharide and disaccharide sugars (cellulose, resistant starch, maltodextrin and sucrose) were replaced with monosaccharides

sugars (fructose and glucose) (MS diet) or, conversely, the monosaccharide sugars were replaced with polysaccharide sugars (PS diet) (7 mice per group divided in 2 cages of 4 and 3 mice). One week after the beginning of the diets, the mice were infected orally with the DBS100 strain of *C. rodentium*.

Statistical analysis

GraphPad Prism version 6.0 was used for all analysis and preparation of graphs. For all data displayed in graphs, the results are expressed as the mean ± s.e.m. For comparisons between two groups, a 2-tailed Student's t test for unpaired data or the nonparametric Mann–Whitney test was used. For comparisons between more than two groups, a one-way analysis of variance (ANOVA) and post hoc Bonferroni test, or the nonparametric Kruskal-Wallis test followed by a post hoc Dunn's test were used. The Kolmogorov-Smirnov test of normality was applied to all data sets, and in cases where the data did not demonstrate a normal distribution, nonparametric tests were used to analyze significant differences. An F or Bartlett's test was performed to determine differences in variances between groups for t tests and ANOVAs, respectively. An unpaired t test with Welch's correction was applied when variances were not equal. Survival between groups of mice was compared using a log rank (Mantel-Cox) test. Differences corresponding to $P < 0.05$ were considered significant.

Acknowledgments We thank the MIMA2 platform for access to IVIS200, which was financed by the Region Ile de France (SESAME), the members of the ANAXEM germ-free platform, the members of the animal facilities of INRA, and T. Ledent of the animal facilities of Saint-Antoine Hospital for their assistance in mouse care; M. Moroldo and J. Lecardonnel from the CRB GADIE core facility for technical assistance in performing the microarray analysis; S. Dumont and F. Merabtene for technical help in histology.

Contributors B.L., M.L.R., M.C. and H.S. conceived and designed the study, analyzed the data, and wrote the manuscript; B.L. designed and conducted all experiments, unless otherwise indicated; V.Z. and M.D. performed the IgG ELISA; H.-P.P. and A.S. conducted the bioinformatics studies and analyzed the microarray experiments; M.-L.M., N.W., J.M.N., G.D.C., J.P., L.D., B.S., and C.B. provided technical help for the *in vivo* experiments; B.L., M.L.R, M.-L.M., N.W., P.L., M.C. and H.S. discussed the experiments and results.

Funding This work was funded by ANR-13-BSV3-0014-01.

Competing interests None declared.

References

1 Nood E van, Vrieze A, Nieuwdorp M, *et al.* Duodenal infusion of donor feces for recurrent Clostridium difficile. *N Engl J Med* 2013;368:407–15.
2 Guo X, Liang Y, Zhang Y, *et al.* Innate Lymphoid Cells Control Early Colonization Resistance against Intestinal Pathogens through ID2-Dependent Regulation of the Microbiota. *Immunity* 2015;42:731–43.
3 Kamada N, Chen GY, Inohara N, *et al.* Control of pathogens and pathobionts by the gut microbiota. *Nat Immunol* 2013;14:685–90.
4 Collins JW, Keeney KM, Crepin VF, *et al.* Citrobacter rodentium: infection, inflammation and the microbiota. *Nat Rev Microbiol* 2014;12:612–23.
5 Kaper JB, Nataro JP, Mobley HL. Pathogenic Escherichia coli. *Nat Rev Microbiol* 2004;2:123–40.
6 Mundy R, MacDonald TT, Dougan G, *et al.* Citrobacter rodentium of mice and man. *Cell Microbiol* 2006;7:1697–706.
7 Jostins L, Ripke S, Weersma RK, *et al.* Host-microbe interactions have shaped the genetic architecture of inflammatory bowel disease. *Nature* 2012;491:119–24.
8 Sokol H, Conway KL, Zhang M, *et al.* Card9 mediates intestinal epithelial cell restitution, T-helper 17 responses, and control of bacterial infection in mice. *Gastroenterology* 2013;145:591–601.e3.
9 Lamas B, Richard ML, Leducq V, *et al.* CARD9 impacts colitis by altering gut microbiota metabolism of tryptophan into aryl hydrocarbon receptor ligands. *Nat Med* 2016;22:598–605.
10 Kamada N, Sakamoto K, Seo S-UU, *et al.* Humoral Immunity in the Gut Selectively Targets Phenotypically Virulent Attaching-and-Effacing Bacteria for Intraluminal Elimination. *Cell Host Microbe* 2015;17:617–27.
11 Mellies JL, Elliott SJ, Sperandio V, *et al.* The Per regulon of enteropathogenic Escherichia coli : identification of a regulatory cascade and a novel transcriptional activator,

the locus of enterocyte effacement (LEE)-encoded regulator (Ler). *Mol Microbiol* 1999;33:296–306.
12 Kamada N, Kim Y-GG, Sham HP, *et al.* Regulated virulence controls the ability of a pathogen to compete with the gut microbiota. *Science* 2012;336:1325–9.
13 Wiles S, Pickard KM, Peng K, *et al.* In vivo bioluminescence imaging of the murine pathogen Citrobacter rodentium. *Infect Imm* 2006;74:5391–6.
14 Segata N, Izard J, Waldron L, *et al.* Metagenomic biomarker discovery and explanation. *Genome Biol* 2011;12:R60.
15 Morgan XC, Tickle TL, Sokol H, *et al.* Dysfunction of the intestinal microbiome in inflammatory bowel disease and treatment. *Genome Biol* 2012;13:R79.
16 El Kaoutari A, Armougom F, Raoult D, *et al.* [Gut microbiota and digestion of polysaccharides]. *Med Sci : M/S* 2014;30:259–65.
17 Macfarlane S, Macfarlane GT. Regulation of short-chain fatty acid production. *The Proc Nutr Soc* 2003;62:67–72.
18 Kim M, Qie Y, Park J, *et al.* Gut Microbial Metabolites Fuel Host Antibody Responses. *Cell Host Microbe* 2016;20:202–14.
19 Ghosh S, Dai C, Brown K, *et al.* Colonic microbiota alters host susceptibility to infectious colitis by modulating inflammation, redox status, and ion transporter gene expression. *Am J Physiol Gastrointest Liver Physiol* 2011;301:G39–49.
20 Bry L, Brigl M, Brenner MB. CD4+-T-cell effector functions and costimulatory requirements essential for surviving mucosal infection with Citrobacter rodentium. *Infect Immun* 2006;74:673–81.
21 Maaser C, Housley MP, Iimura M, *et al.* Clearance of Citrobacter rodentium requires B cells but not secretory immunoglobulin A (IgA) or IgM antibodies. *Infect Immun* 2004;72:3315–24.
22 Pickert G, Neufert C, Leppkes M, *et al.* STAT3 links IL-22 signaling in intestinal epithelial cells to mucosal wound healing. *J Exp Med* 2009;206:1465–72.
23 Rutz S, Eidenschenk C, Ouyang W. IL-22, not simply a Th17 cytokine. *Immunol Rev* 2013;252:116–32.
24 Sonnenberg GF, Fouser LA, Artis D. Border patrol: regulation of immunity, inflammation and tissue homeostasis at barrier surfaces by IL-22. *Nat Immunol* 2011;12:383–90.
25 Stelter C, Käppeli R, König C, *et al.* Salmonella-induced mucosal lectin RegIIIβ kills competing gut microbiota. *PLoS One* 2011;6:e20749.
26 Ishigame H, Kakuta S, Nagai T, *et al.* Differential roles of interleukin-17A and -17F in host defense against mucoepithelial bacterial infection and allergic responses. *Immunity* 2009;30:108–19.
27 Zheng Y, Valdez PA, Danilenko DM, *et al.* Interleukin-22 mediates early host defense against attaching and effacing bacterial pathogens. *Nat Med* 2008;14:282–9.
28 Willing BP, Vacharaksa A, Croxen M, *et al.* Altering host resistance to infections through microbial transplantation. *PLoS One* 2011;6:e26988. doi:10.1371/journal.pone.0026988
29 Ivanov II, Atarashi K, Manel N, *et al.* Induction of intestinal Th17 cells by segmented filamentous bacteria. *Cell* 2009;139:485–98.
30 Hara H, Ishihara C, Takeuchi A, *et al.* The adaptor protein CARD9 is essential for the activation of myeloid cells through ITAM-associated and Toll-like receptors. *Nat Immunol* 2007;8:619–29.

Figure Legends

Figure 1 CARD9 is involved in the control of *C. rodentium* virulence. (A) *C. rodentium* count in feces (left) and area under the curve (AUC) (right) based in *C. rodentium* count in feces of WT and *Card9*$^{-/-}$ mice (n=6) infected orally with 1 x 10^9 CFU of the DBS100 strain of *C. rodentium.* (B) Weight of WT and *Card9*$^{-/-}$ mice (n=6) infected with *C. rodentium*. (C) Lipocalin levels in the feces of WT and *Card9*$^{-/-}$ mice (n=6) infected with *C. rodentium*. (D) Concentration of *C. rodentium*-specific IgG in the feces of WT and *Card9*$^{-/-}$ mice (n=6) infected with *C. rodentium*. (E) Expression of *ler* in the feces of WT and *Card9*$^{-/-}$ mice (n=6) infected with *C. rodentium*. The results show *ler* expression normalized to the expression of 16S rDNA genes. The data are expressed as the mean ± SEM. *p < 0.05; **p < 0.01 by the Student's t test (A, B, D and E) or by Mann-Whitney U test (C).

Figure 2 GF *Card9*$^{-/-}$ mice exhibit impaired control of phenotypically virulent *C. rodentium* through a defective humoral response. (A) Bacterial burden in the fecal pellets of GF WT and GF *Card9*$^{-/-}$ mice (n=6) infected with *C. rodentium*. (B) Lipocalin levels in the feces of GF WT and GF *Card9*$^{-/-}$ mice (n=6) infected with *C. rodentium*. (C and D) Representative images of H&E-stained colons at post-infection day 4 (C) and the histological scores (D) of GF WT and GF *Card9*$^{-/-}$ mice (n=6) infected with *C. rodentium*. Scale bars represent 200 µm. (E) Production of *C. rodentium*-specific IgG in the feces of GF WT and GF *Card9*$^{-/-}$ mice (n=6) during the infection. (F) Expression of *ler* in the feces of GF WT and GF *Card9*$^{-/-}$ mice (n=6) infected with *C. rodentium*. The results show *ler* expression (1/*Ct*) normalized by the CFU of *C. rodentium* in the same samples. The data are expressed as the mean ± SEM. *p < 0.05; **p < 0.01; ***p < 0.001 by the Mann-Whitney U test (B, D and E) or by the Student's t test (F).

Figure 3 Transfer of the microbiota of *Card9*$^{-/-}$ mice is sufficient to increase susceptibility to *C. rodentium*-induced colitis. (A) Germ-free WT mice colonized with the microbiota of WT (WT→GF) or *Card9*$^{-/-}$ (*Card9*$^{-/-}$→GF) mice (n=10) were infected orally with 1 x 10^9 CFU of *C. rodentium*, and the pathogen load was assessed by CFU counts in fecal samples. (B) Lipocalin levels in the feces of WT→GF and *Card9*$^{-/-}$→GF mice (n=10) infected with *C. rodentium*. (C and D) Representative images of H&E-stained colons at post-infection day 12 (C) and the histological scores (D) of WT→GF and *Card9*$^{-/-}$→GF mice (n=10) infected with *C. rodentium*. Scale bars represent 200 μm. (E) Comparative expression of genes in the cecum by microarray analysis (log2-transformed (fold change compared to day 0 expression levels)) on day 4 after infection of WT→GF and *Card9*$^{-/-}$→GF mice (n=5) with *C. rodentium*. (F) *Il22*, *Reg3g*, *Reg3b* and *Il17a* transcript expression in the cecum before (day 0, n=5) and after (day 4, day 12 and day 22, n=5) infection of WT→GF and *Card9*$^{-/-}$→GF mice with *C. rodentium*. (G) Amounts of IL-22 secreted by MLN cells from WT→GF and *Card9*$^{-/-}$→GF mice (n=5) infected with *C. rodentium.* (H) Expression of *ler* in the feces of WT→GF and *Card9*$^{-/-}$→GF mice (n=10) infected with *C. rodentium*. The results show *ler* expression normalized to the expression of 16S rDNA genes. The data are expressed as the mean ± SEM. The results are representative of at least two experiments (A, B and D). *$p < 0.05$; **$p < 0.01$; ***$p < 0.001$ by the Student's t test (A, B, D, F and G) or the Mann-Whitney U test (H).

Figure 4 The bacterial microbiota of *Card9*$^{-/-}$ mice is altered and could preferentially uses polysaccharides over monosaccharides. (A) Principal component analysis based on the bacterial 16S rDNA gene sequence abundance in fecal content from WT→GF and *Card9*$^{-/-}$→GF mice (n=5) infected with *C. rodentium*. The axes correspond to principal components 1 (x-axis), 2 (y-axis) and 3 (z-axis). P value calculated by ANOSIM (9999 permutations) (B)

Pairwise Beta diversity distance in the fecal samples of WT→GF and *Card9*$^{-/-}$→GF mice (n=5) infected with *C. rodentium*. *p < 0.05; ***p < 0.001 by ANOVA with a *post hoc* Bonferroni test. (C) Bacterial-taxon-based analysis at the phylum level in the feces from WT→GF and *Card9*$^{-/-}$→GF mice (n=5) infected with *C. rodentium*. (D) Bacterial diversity based on the Shannon index in the fecal samples from WT→GF and *Card9*$^{-/-}$→GF mice (n=5) infected with *C. rodentium*. The dots represent individual mice, and the horizontal line indicates the mean. **p < 0.01; ns, not significant by the Student's t test. (E) Bacterial taxa differentially enriched in WT→GF and *Card9*$^{-/-}$→GF mice (n=5) before infection (day 0) (generated using the LEfSe pipeline). The heat map shows the relative abundance of taxa. Only significant differences with linear differential analysis (LDA) scores > 2 are shown. (F) Sugar metabolism pathways differentially enriched in WT→GF and *Card9*$^{-/-}$→GF mice (n=5) before infection (day 0) (inferred metagenomics using Picrust software).

Figure 5 Effects of the MSs and PS diets on the gut microbiota of WT and *Card9*$^{-/-}$ mice. (A) Principal component analysis based on the bacterial 16S rDNA gene sequence abundance in fecal content from WT and *Card9*$^{-/-}$ mice (n=7) before infection. The mice were fed either a monosaccharide (MS) or polysaccharide (PS) diet for 1 week. The axes correspond to principal components 1 (x-axis), 2 (y-axis) and 3 (z-axis), **p < 0.01; ***p < 0.001 (ANOSIM, 9999 permutations). (B) Bacterial diversity based on the Shannon index in the fecal samples from WT and *Card9*$^{-/-}$ mice (n=7) fed the MS or PS diet. The dots represent individual mice, and the horizontal line indicates the mean. The data are expressed as the mean ± SEM. ***p <0.001 by ANOVA with a *post hoc* Bonferroni test. (C) Differences in abundance are shown for the bacterial taxa in WT and *Card9*$^{-/-}$ mice (n=7) fed the PS diet (generated using the LEfSe pipeline).

Figure 6 Polysaccharide diet overrides the susceptibility of *Card9*$^{-/-}$ mice to *C. rodentium*. (A) *C. rodentium* count in feces (left) and weight (right) of WT and *Card9*$^{-/-}$ mice (n=6). The mice were fed either a monosaccharide (MS) or polysaccharide (PS) diet, and 1 week after the beginning of the diets, the mice were infected orally with 1 x 10^9 CFU of *C. rodentium*. For statistical comparisons, § indicates WT MSs versus *Card9*$^{-/-}$ MSs; * indicates *Card9*$^{-/-}$ MSs versus *Card9*$^{-/-}$ PSs. (B) Lipocalin levels in the feces of WT and *Card9*$^{-/-}$ mice (n=6) fed either the MS or PS diet and infected with *C. rodentium*. For statistical comparisons, § indicates WT MSs versus *Card9*$^{-/-}$ MSs; * indicates *Card9*$^{-/-}$ MSs versus *Card9*$^{-/-}$ PSs; † indicates WT MSs versus WT PSs. (C and D) Representative images of H&E-stained colons at post-infection day 22 (C) and histological scores (D) of WT and *Card9*$^{-/-}$ mice (n=6) that were fed either the MS or PS diet and infected with *C. rodentium*. Scale bars represent 200 µm. (E) Production of *C. rodentium*-specific IgG in the feces of WT and *Card9*$^{-/-}$ mice (n=6) that were fed either the MS or PS diet and infected with *C. rodentium*. For statistical comparisons, * indicates *Card9*$^{-/-}$ MSs versus *Card9*$^{-/-}$ PSs; † indicates WT MSs versus WT PSs. (F) Expression of *ler* in the feces of WT and *Card9*$^{-/-}$ mice (n=6) that were fed either the MS or PS diet and infected with *C. rodentium*. The results show *ler* expression normalized to the expression of 16S rDNA genes. The data are expressed as the mean ± SEM. *$p < 0.05$; $^{§}p < 0.05$; $^{†}p < 0.05$; **$p < 0.01$; $^{§§}p < 0.01$; ***$p < 0.001$ by the Student's t test (E) or by ANOVA with a *post hoc* Bonferroni test (A, B, D and F).

Figure 7 Proposed model illustrating the gut microbiota-dependent and -independent role of CARD9 in the response to *C. rodentium* infection. CARD9 controls pathogen virulence in a microbiota-independent manner by supporting a specific humoral response and shapes also the microbiota inducing a competition for sugar with pathogens. These mechanisms lead to pathogens elimination.

Figure 1

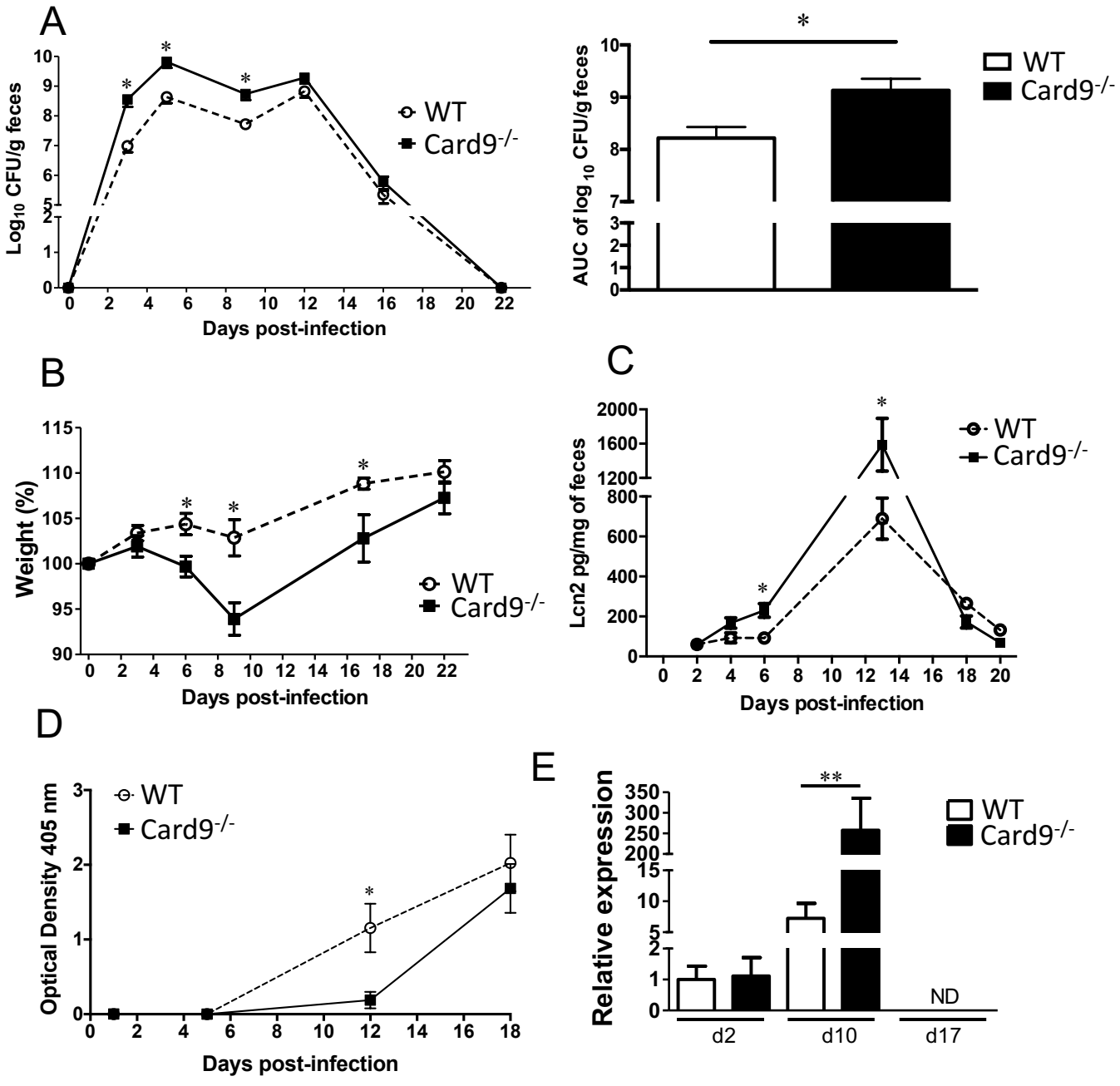
A
Log10 CFU/g feces
Days post-infection
WT
Card9-/-
AUC of log 10 CFU/g feces
B
Weight (%)
C
Lcn2 pg/mg of feces
D
Optical Density 405 nm
E
Relative expression
ND
d2
d10
d17

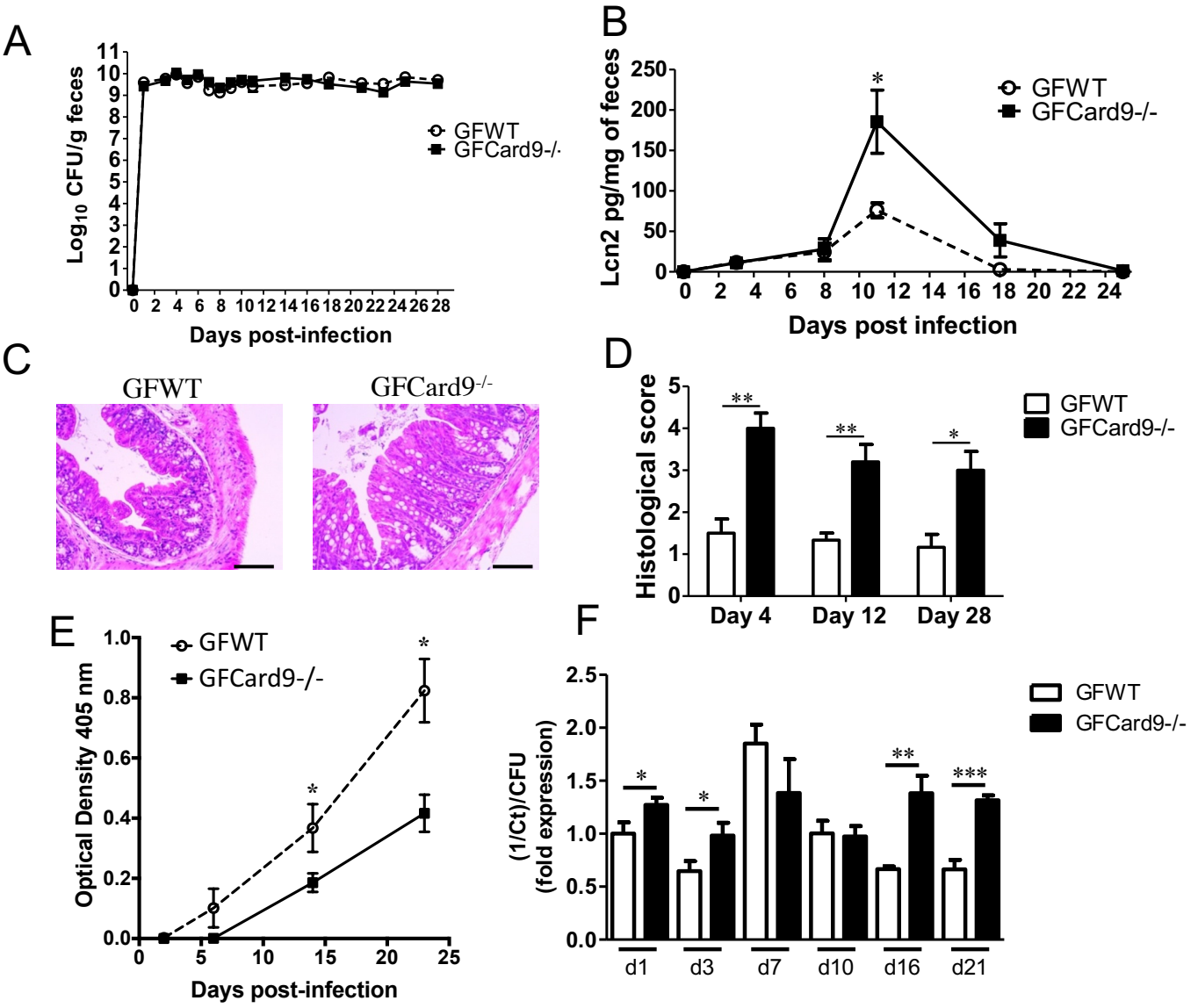
A
Log10 CFU/g feces
Days post-infection
GFWT
GFCard9-/-
B
Lcn2 pg/mg of feces
Days post infection
GFWT
GFCard9-/-
C
GFWT
GFCard9-/-
D
Histological score
Day 4
Day 12
Day 28
GFWT
GFCard9-/-
E
Optical Density 405 nm
Days post-infection
GFWT
GFCard9-/-
F
(1/Ct)/CFU
(fold expression)
d1
d3
d7
d10
d16
d21
GFWT
GFCard9-/-

Figure 3

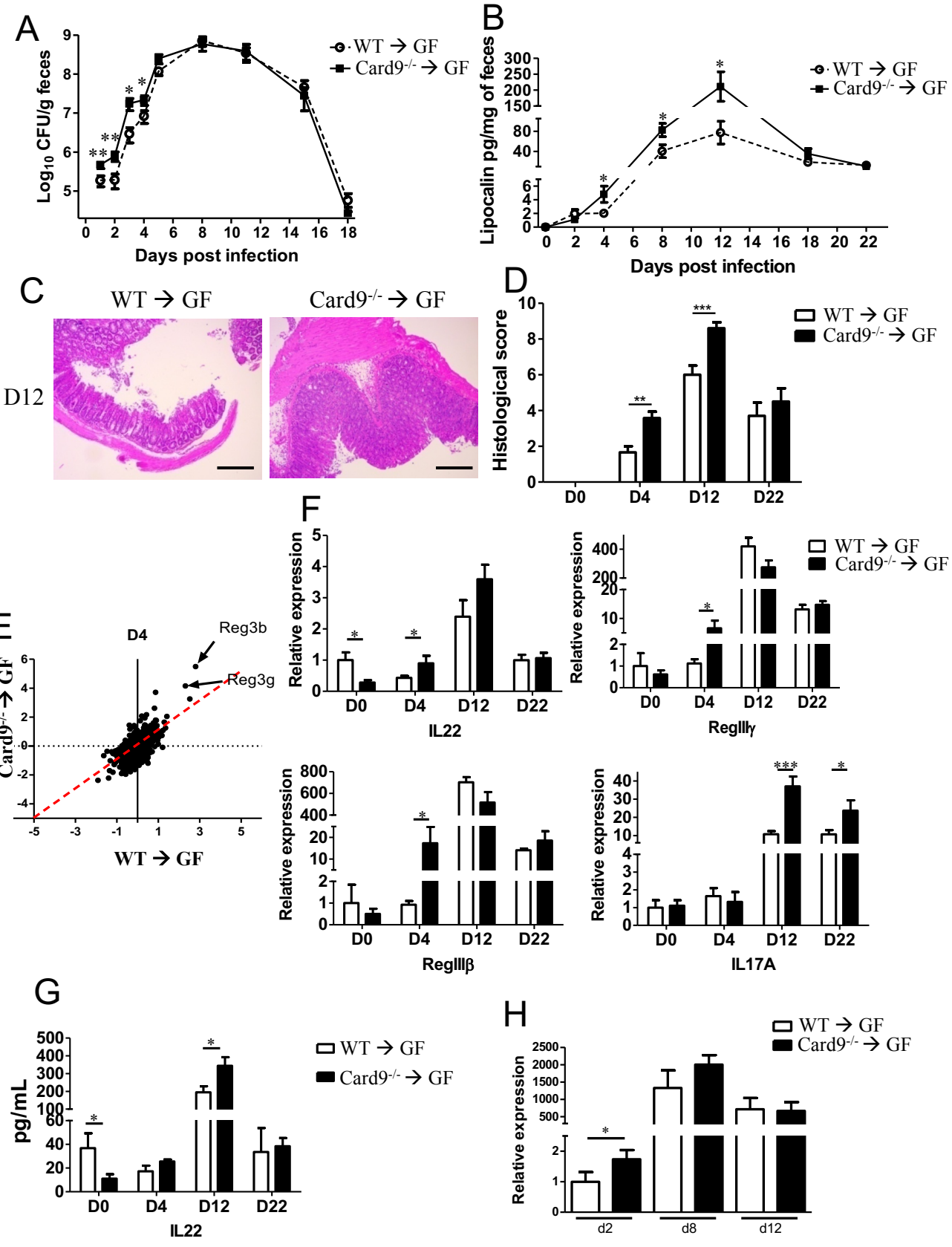
A
Log10 CFU/g feces
Days post infection
WT → GF
Card9-/- → GF
B
Lipocalin pg/mg of feces
Days post infection
WT → GF
Card9-/- → GF
C
WT → GF
Card9-/- → GF
D12
D
Histological score
WT → GF
Card9-/- → GF
D0
D4
D12
D22
E
D4
Reg3b
Reg3g
Card9-/- → GF
WT → GF
F
Relative expression
IL22
RegIIIγ
RegIIIβ
IL17A
WT → GF
Card9-/- → GF
G
pg/mL
IL22
WT → GF
Card9-/- → GF
H
Relative expression
d2
d8
d12
WT → GF
Card9-/- → GF

Figure 4

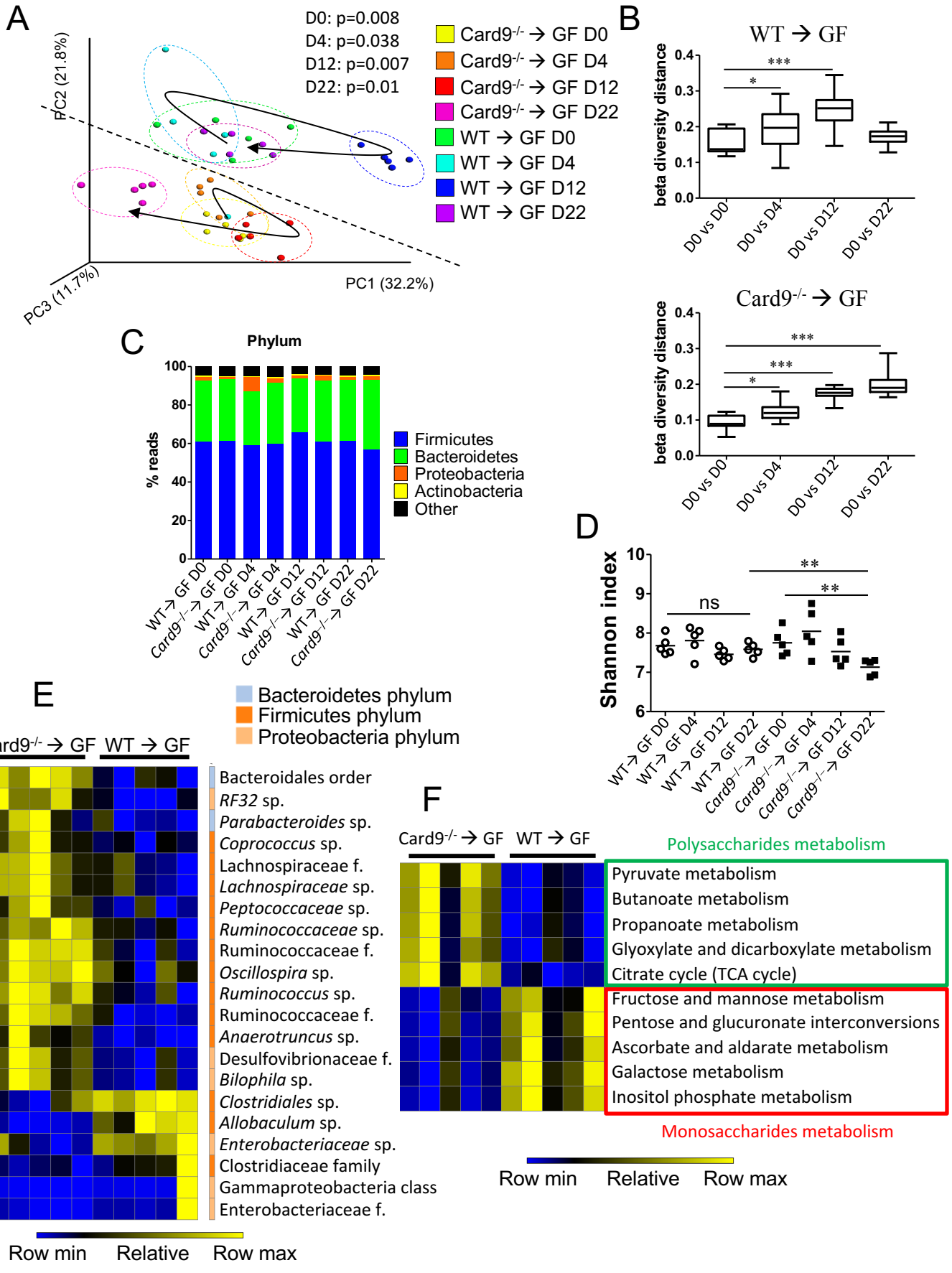
A
D0: p=0.008
D4: p=0.038
D12: p=0.007
D22: p=0.01
Card9-/- → GF D0
Card9-/- → GF D4
Card9-/- → GF D12
Card9-/- → GF D22
WT → GF D0
WT → GF D4
WT → GF D12
WT → GF D22
PC2 (21.8%)
PC1 (32.2%)
PC3 (11.7%)
B
WT → GF
Card9-/- → GF
beta diversity distance
D0 vs D0
D0 vs D4
D0 vs D12
D0 vs D22
C
Phylum
% reads
Firmicutes
Bacteroidetes
Proteobacteria
Actinobacteria
Other
D
Shannon index
ns
E
Bacteroidetes phylum
Firmicutes phylum
Proteobacteria phylum
Card9-/- → GF
WT → GF
Bacteroidales order
RF32 sp.
Parabacteroides sp.
Coprococcus sp.
Lachnospiraceae f.
Lachnospiraceae sp.
Peptococcaceae sp.
Ruminococcaceae sp.
Ruminococcaceae f.
Oscillospira sp.
Ruminococcus sp.
Ruminococcaceae f.
Anaerotruncus sp.
Desulfovibrionaceae f.
Bilophila sp.
Clostridiales sp.
Allobaculum sp.
Enterobacteriaceae sp.
Clostridiaceae family
Gammaproteobacteria class
Enterobacteriaceae f.
Row min
Relative
Row max
F
Polysaccharides metabolism
Pyruvate metabolism
Butanoate metabolism
Propanoate metabolism
Glyoxylate and dicarboxylate metabolism
Citrate cycle (TCA cycle)
Fructose and mannose metabolism
Pentose and glucuronate interconversions
Ascorbate and aldarate metabolism
Galactose metabolism
Inositol phosphate metabolism
Monosaccharides metabolism

Figure 5

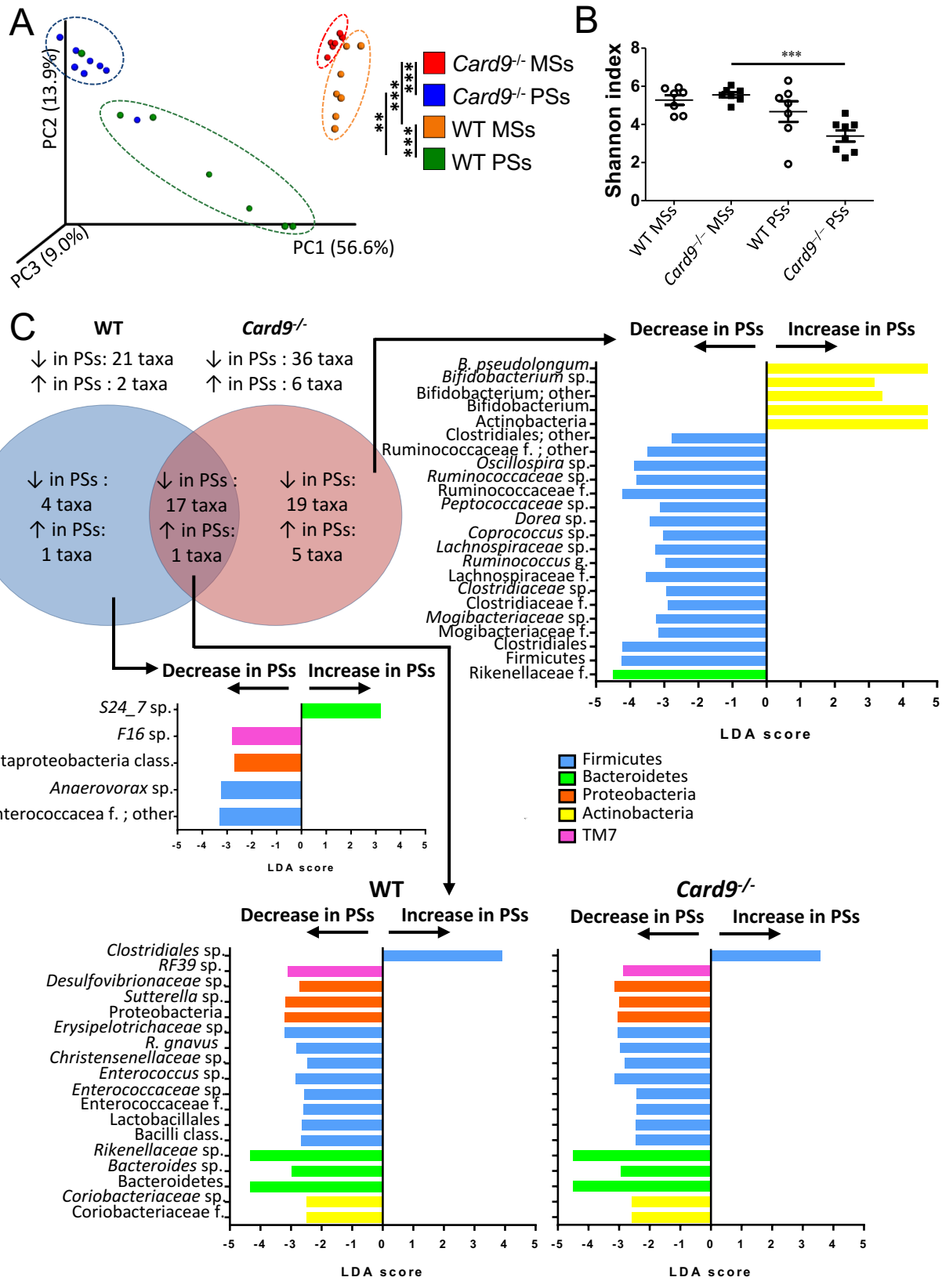
A
PC2 (13.9%)
PC3 (9.0%)
PC1 (56.6%)
Card9-/- MSs
Card9-/- PSs
WT MSs
WT PSs
B
Shannon index
WT MSs
Card9-/- MSs
WT PSs
Card9-/- PSs
C
WT
Card9-/-
↓ in PSs: 21 taxa
↑ in PSs : 2 taxa
↓ in PSs : 36 taxa
↑ in PSs : 6 taxa
↓ in PSs : 4 taxa ↑ in PSs: 1 taxa
↓ in PSs : 17 taxa ↑ in PSs: 1 taxa
↓ in PSs: 19 taxa ↑ in PSs: 5 taxa
Decrease in PSs
Increase in PSs
B. pseudolongum
Bifidobacterium sp.
Bifidobacterium; other
Bifidobacterium
Actinobacteria
Clostridiales; other
Ruminococcaceae f. ; other
Oscillospira sp.
Ruminococcaceae sp.
Ruminococcaceae f.
Peptococcaceae sp.
Dorea sp.
Coprococcus sp.
Lachnospiraceae sp.
Ruminococcus g.
Lachnospiraceae f.
Clostridiaceae sp.
Clostridiaceae f.
Mogibacteriaceae sp.
Mogibacteriaceae f.
Clostridiales
Firmicutes
Rikenellaceae f.
LDA score
S24_7 sp.
F16 sp.
Deltaproteobacteria class.
Anaerovorax sp.
Enterococcacea f. ; other
Firmicutes
Bacteroidetes
Proteobacteria
Actinobacteria
TM7
Clostridiales sp.
RF39 sp.
Desulfovibrionaceae sp.
Sutterella sp.
Proteobacteria
Erysipelotrichaceae sp.
R. gnavus
Christensenellaceae sp.
Enterococcus sp.
Enterococcaceae sp.
Enterococcaceae f.
Lactobacillales
Bacilli class.
Rikenellaceae sp.
Bacteroides sp.
Bacteroidetes
Coriobacteriaceae sp.
Coriobacteriaceae f.

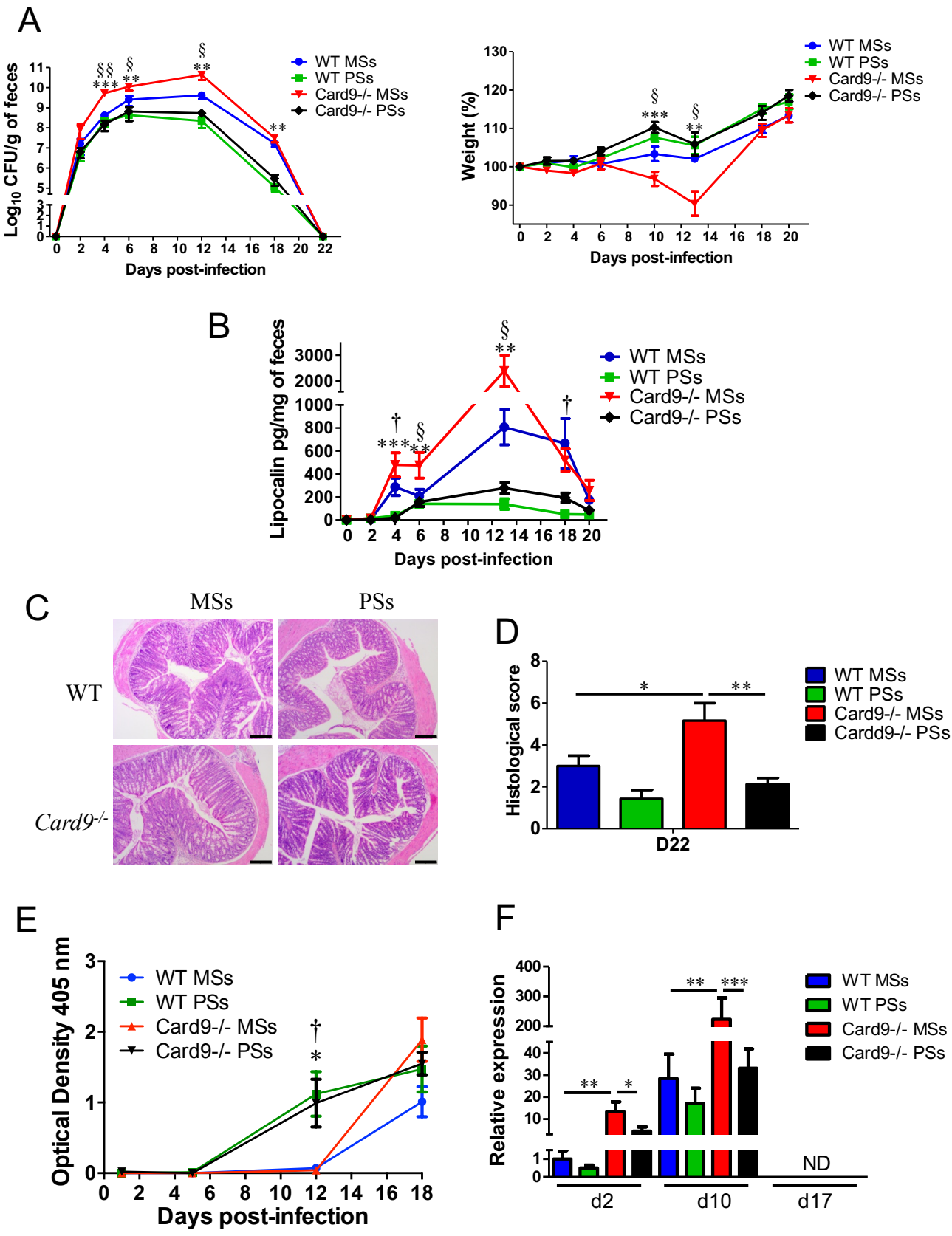
A
Log10 CFU/g of feces
Days post-infection
WT MSs
WT PSs
Card9-/- MSs
Card9-/- PSs
Weight (%)
Days post-infection
B
Lipocalin pg/mg of feces
Days post-infection
C
MSs
PSs
WT
Card9-/-
D
Histological score
D22
Cardd9-/- PSs
E
Optical Density 405 nm
Days post-infection
F
Relative expression
ND
d2
d10
d17

Figure 7

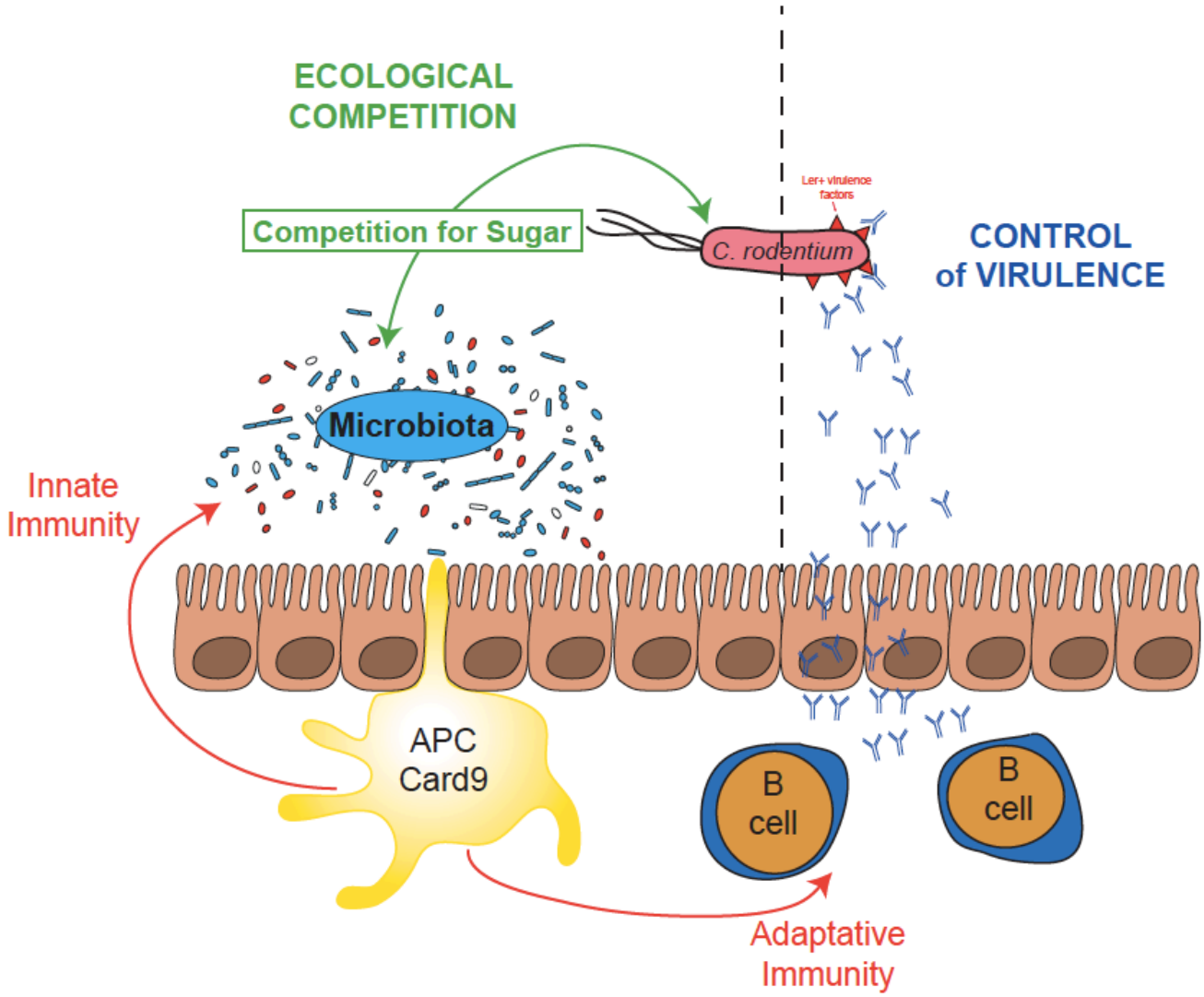
ECOLOGICAL
COMPETITION
Competition for Sugar
Ler+ virulence factors
C. rodentium
CONTROL
of VIRULENCE
Microbiota
Innate
Immunity
APC
Card9
B
cell
B
cell
Adaptative
Immunity

SUPPLEMENTARY MATERIAL

SUPPLEMENTARY METHODS

***In vivo* bioluminescence measurement**

Mice were anesthetized and bioluminescence was measured using the IVIS 200 imaging system (Xenogen). Living Image software (version 4.0, Caliper Life Sciences) was used to measure the luciferase activities. For colon and cecum bioluminescence measurement, mice were killed by cervical dislocation and the colon and the cecum were removed to a sterile petri dish. Bioluminescence images were acquired for 1 min with f/stop=1 and binning=4. A digital false-colour photon emission of the mouse or the organ was generated, and photons were counted within a constant region of interest. Photon emission was measured as radiance in photons/s/cm^2/sr. For feces bioluminescence, fecal pellets were suspended in PBS at 30mg/mL, and luminescence emitted from *C. rodentium* was measured using Infinite M200 PRO luminometer (TECAN).

Gut microbiota transfer

Fresh stool samples from WT or *Card9*$^{-/-}$ mice (8 weeks old, male) were immediately transferred to an anaerobic chamber, in which the stool samples were suspended and diluted in LYHBHI medium (BD Difco, Le Pont De Claix, France) supplemented with cellobiose (1 mg/ml; Sigma-Aldrich, St. Louis, MO, USA), maltose (1 mg/ml; Sigma-Aldrich), and cysteine (0.5 mg/ml; Sigma-Aldrich). WT germ-free mice (4-5 weeks old, female) were randomly assigned to two groups (4 cages with 5 mice per cage in 2 different isolators) and inoculated via oral gavage with 400 µl of a fecal suspension (1:100) from the conventional wild-type (WT→GF) or *Card9*$^{-/-}$ (*Card9*$^{-/-}$→GF) mice. One aliquot of each fecal suspension was stored at -80°C. All experiments in WT→GF and *Card9*$^{-/-}$→GF mice were performed three weeks after inoculation. Fresh stools from WT→GF or *Card9*$^{-/-}$→GF mice were

randomly taken in each cage of each isolator before (day 0, n=5) and during *C. rodentium*-induced colitis (day 4, 12 and 22, n=5) for microbiota analysis.

Custom rodent diet experiment

WT and *Card9*$^{-/-}$ mice were randomly assigned to two groups (7 mice in each group: 7 mice divided in 2 cages of 4 and 3 mice) and fed either MS diet (WT MSs, *Card9*$^{-/-}$MSs) or PS diet (WT PSs, *Card9*$^{-/-}$PSs).

Quantification of cytokines

MLNs were sieved through a 70-µm cell strainer (BD) in complete RPMI 1640 medium (10% heat-inactivated fetal calf serum, 2 mM L-glutamine, 50 IU/ml penicillin, and 50 µg/ml streptomycin; Sigma-Aldrich), and 1 x 10^6 cells per well were cultured (37°C, 10% CO_2) for 48 h with stimulation by phorbol 12-myristate 13-acetate (PMA, 50 ng/ml; Sigma-Aldrich) and ionomycin (1 µM; Sigma-Aldrich). All collected supernatants were frozen at -80°C until processing. The quantification of mouse cytokines was performed by ELISA according to the manufacturer's instructions: IL-22 (eBioscience).

Quantification of fecal lipocalin-2 (Lcn2)

Frozen fecal samples were reconstituted in PBS and vortexed to get a homogenous fecal suspension. These samples were centrifuged for 5 min at 10 000g and 4°C. Supernatants were collected and stored at -20°C until analysis. ELISA was performed by using DuoSet® ELISA Development Systems for Lcn2 (DY1857) from R&D Systems according to manufacturer's instructions.

Determination of *C. rodentium*-specific antibody responses.

A culture of *C. rodentium* (OD_{600}=1) was heat killed at 60°C for 1.5 h and frozen at -80°C until processing. Corning™ Costar™ 96-Well Half-Area flat bottom plates were coated with

0.1% poly-L-lysine (Sigma-Aldrich) and dried for 1 h at 60°C. The heat killed *C. rodentium* was added to the 96-well plates and incubated at 4°C overnight. The next day, the heat killed *C. rodentium* was fixed by adding 10% PFA (Sigma-Aldrich) for 30 min. The plates were then washed 3 times with PBS containing 0.05% Tween (Sigma-Aldrich) and blocked with PBS containing 1% BSA (Sigma-Aldrich), for 1 h. Fecal supernatants were added to the plates, and the presence of *C. rodentium*-specific Igs was detected by alkaline phosphatase-conjugated polyclonal anti-mouse IgG antibodies (Sigma-Aldrich). The plates were developed using p-nitrophenyl phosphate substrate (Mabtech), and the OD_{405} values were determined.

Histology

Colon samples for histological studies were maintained at 4°C in 4% paraformaldehyde and then embedded in paraffin. Sections (4 μm thick) were stained with hematoxylin and eosin (H&E) and then examined blindly using a BX43 Olympus microscope to determine the histological score according to previously described methods with some modifications.[1]In brief, the system assessed submucosal edema, epithelial hyperplasia, goblet cell depletion, and epithelial integrity. The combined pathological score ranged from 0 to 13 arbitrary units.

Gene expression analysis using quantitative reverse-transcription PCR (qRT-PCR)

Total RNA was isolated from cecum samples using an RNeasy Mini Kit (Qiagen) according to the manufacturer's instructions. To measure *ler* expression, total RNA was isolated from fecal samples using a High Pure Isolation Kit (Roche) with an improved protocol described previously.[2]Quantitative RT-PCR was performed using SuperScript II Reverse Transcriptase (Life Technologies) and then a TaqMan Gene Expression Assay (Life Technologies) for the quantification of all bacterial sequences or a Takyon SYBR Green PCR kit (Eurogentec) for the quantification of all other genes. qRT-PCR was performed using a StepOnePlus apparatus (Applied Biosystems) with specific oligonucleotides. The

oligonucleotides used were as follows: *Gapdh*, 5′-AACTTTGGCATTGTGGAAGG-3′ and 5′-ACACATTGGGGGTAGGAACA-3′; *Il17A*, 5′-TTTAACTCCCTTGGCGCAAAA-3′ and 5′-CTTTCCCTCCGCATTGACAC-3′; *Il22*, 5′-CATGCAGGAGGTGGTACCTT-3′ and 5′-CAGACGCAAGCATTTCTCAG-3′; *Reg3g*, 5′-TTCCTGTCCTCCATGATCAAAA-3′ and 5′-CATCCACCTCTGTTGGGTTCA-3′; *Reg3b*, 5′-ATGCTGCTCTCCTGCCTGATG-3′ and 5′-CTAATGCGTGCGGAGGGTATATTC-3′; and *ler*, 5′-AATATACCTGATGGTGCTCTTG-3′ and 5′-TTCTTCCATTCAATAATGCTTCTT-3′. The probes and the primers for the bacterial 16S rDNA genes were described previously.[3]For cecal gene expression, we used the $2^{-\Delta\Delta Ct}$ quantification method with mouse *Gapdh* as an endogenous control and the WT→GF group as a calibrator. The qRT-PCR results for *ler* were normalized to the expression of 16S rDNA genes or to the CFU of *C. rodentium* in the same samples, and the WT→GF, WT, WT MSs or GF WT group was used as a calibrator.

Lamina propria cell isolation and flow cytometry

Cells from the colon lamina propria were isolated as previously described.[4]The cells were stained as previously described. [5] The following antibodies were used for surface staining of: CD19 (6D5, eBioscience); CD69 (H1.2F3, Biolegend); CD5 (53-7.3, Biolegend); IgD (11-26c.2a, Biolegend); IgM (RMM-1, Biolegend); major histocompatibility complex (MHC) II (M5/114.15.2, eBioscience). Flow cytometry was carried out by BD-Fortessa. Data were analyzed by using FlowJo software.

16S rRNA gene sequencing

DNA of cecal content was extracted from the weighted cecal content samples of mice before and during the infection as previously described.[3]For the bead beating step, we used 0.1-mm diameter silica beads with 0.6-mm diameter beads. Microbial diversity was determined for each sample by targeting a portion of the ribosomal genes. A 16S rRNA gene fragment

comprising V3 and V4 hypervariable regions (16S; 5′-TACGGRAGGCAGCAG-3′ and 5′-CTACCNGGGTATCTAAT-3′) was amplified using an optimized and standardized 16S-amplicon-library preparation protocol (Metabiote, GenoScreen). Briefly, 16S rRNA gene PCR was performed using 5 ng genomic DNA according to the manufacturer's protocol (Metabiote) using 192 bar-coded primers (Metabiote MiSeq Primers, GenoScreen) at final concentrations of 0.2 μM and an annealing temperature of 50°C for 30 cycles. The PCR products were purified using an Agencourt AMPure XP-PCR Purification system (Beckman Coulter), quantified according to the manufacturer's protocol, and multiplexed at equal concentrations. Sequencing was performed using a 300-bp paired-end sequencing protocol on an Illumina MiSeq platform (Illumina) at GenoScreen. Raw paired-end reads were subjected to the following process: (1) quality filtering using the PRINSEQ-lite PERL script[6]by truncating the bases from the 3′ end that did not exhibit a quality < 30 based on the Phred algorithm; (2) paired-end read assembly using FLASH[7](fast length adjustment of short reads to improve genome assemblies) with a minimum overlap of 30 bases and a 97% overlap identity; and (3) searching and removing both forward and reverse primer sequences using CutAdapt, with no mismatches allowed in the primers sequences. Assembled sequences for which perfect forward and reverse primers were not found were eliminated.

16S rRNA gene sequence analysis

The sequences were demultiplexed and quality filtered using the Quantitative Insights Into Microbial Ecology (QIIME, version 1.8.0) software package,[8]and the forward and reverse Illumina reads were joined using the fastq-join method (http://code.google.com/p/ea-utils). The sequences were assigned to OTUs using the UCLUST algorithm[9]with a 97% threshold of pairwise identity and classified taxonomically using the Greengenes reference database.[10]Principal component analysis of the Bray Curtis distance were built and used to assess the variation between experimental groups (beta diversity). Significativity was assessed

using ANOSIM (9999 permutations). The number of observed species and the Shannon diversity index were calculated using rarefied data (depth = 19,000 sequences/sample for WT→GF and *Card9*$^{-/-}$→GF mice and 6,000 sequences/sample for the MS and PS experiment) and used to characterize species diversity in a community. The sequencing data were deposited in the European Nucleotide Archive under accession number PRJEB18666.

Gene expression by microarray analysis

Total RNA was isolated using the protocol described above. RNA integrity was verified using a Bioanalyser 2100 with RNA 6000 Nano chips (Agilent Technologies). Transcriptional profiling was performed on mouse colon samples using the SurePrint G3 Mouse GE 8x60K Microarray kit (Design ID: 028005, Agilent Technologies). Cyanine-3 (Cy3)-labeled cRNAs were prepared with 100 ng of total RNA using a One-Color Low Input Quick Amp Labeling kit (Agilent Technologies) following the recommended protocol. The specific activities and cRNA yields were determined using a NanoDrop ND-1000 (Thermo Fisher Scientific). For each sample, 600 ng of Cy3-labeled cRNA (specific activity > 11.0 pmol Cy3/µg of cRNA) were fragmented at 60°C for 30 min and hybridized to the microarrays for 17 h at 65°C in a rotating hybridization oven (Agilent Technologies). After hybridization, the microarrays were washed and then immediately dried. After washing, the slides were scanned using a G2565CA Scanner System (Agilent Technologies) at a resolution of 3 µm and a dynamic range of 20 bits. The resulting TIFF images were analyzed using the Feature Extraction Software v10.7.3.1 (Agilent Technologies) according to the GE1_107_Sep09 protocol. The microarray data were submitted to GEO under accession number GSE90577.

Microarray analysis

Agilent Feature Extraction software was used to convert the scanned signals into tab-delimited text that could be analyzed using third-party software. The R package *agilp* was used to pre-process the raw data. Box plots and PCAs were used to obtain a general overview

of the data in terms of the within-array distributions of signals and between-sample variability. The Agilent Feature Extraction software computed a *P* value for each probe in each array to test whether the scanned signals were significantly higher than the background signal. The null hypothesis was "the measured signal is equal to background signal." Detected probes were considered if the *P* value was lower than 0.05. The probes must have been present in at least 60% of the samples in each group and under at least one condition to be considered for analysis. To compare data from multiple arrays, the data were normalized to minimize the effect of non-biological differences. Quantile normalization[11]is a method that can quickly normalize within a set of samples without using a reference base. After normalization, spike-in, positive and negative control probes were removed from the normalized data. For the differential expression analysis, we used the limma eBayes test,[12]which finds a compromise between the variance estimate for the gene under consideration and the average variance of all the genes. The Benjamini-Hochberg correction method was used to control the false discovery rate (FDR). All significant gene lists were annotated for enriched biological functions and pathways using the DAVID platform[13,14]for gene ontology (GO) and Kyoto Encyclopedia of Genes and Genomes (KEGG) terms. Significant canonical pathways had adjusted *P* values, according to Benjamini's method, below 0.05. We used Venn diagrams to globally visualize the overlap between all significant genes in the WT and *Card9*$^{-/-}$ comparisons. Thus, DAVID was used to test for the biological pathway enrichment of the Venn elements.

SUPPLEMENTAL FIGURE LEGENDS

Supplementary figure S1 CARD9 is required for the protection from *C. rodentium* infection. (A) Whole body imaging of WT and *Card9*$^{-/-}$ mice infected orally with 1 x 10^9 CFU of the luminescent strain of *C. rodentium* (strain ICC180) and imaged at the indicated

days post-infection. (B) Graph of luminescence in mice. Luminescence was quantified using the region-of-interest tool in the Living Image software (n=6). (C) Bacterial burden in fecal pellets of WT and *Card9*$^{-/-}$ mice (n=6) infected with luminescent strain of *C. rodentium*. Luminescence of feces diluted in PBS was quantified at the indicated day post-infection. (D) Representative bioluminescence in cecum (left) and colon (right) of WT and *Card9*$^{-/-}$ mice infected with luminescent strain of *C. rodentium*. Imaging was performed on day 4 and 12 post-infection. (E and F) Graph of luminescence in cecum (E) and colon (F) (n=6). Luminescence was quantified using the region-of-interest tool in the Living Image software. Data expressed as mean ± SEM. *p < 0.05; **p<0.01 by Student's t test. Results are representative of six individual mice in each group (A and D).

Supplementary figure S2 Quantification of B cells isolated from colon lamina propria of WT and *Card9*$^{-/-}$ mice at baseline. (A) Representative flow cytometry analysis (left) and proportion (right) of B cells ($CD19^+$ $MHCII^+$, among the lymphocyte gate) isolated from colon lamina propria of WT and *Card9*$^{-/-}$ mice at baseline (n=5). (B) Representative flow cytometry analysis (left) and proportion (right) of immature (IgM^- IgD^-), transitional (IgM^+ IgD^-) and early (IgM^+ IgD^+) and late mature (IgM^- IgD^+) cells among B lymphocytes isolated from colon lamina propria of WT and *Card9*$^{-/-}$ mice at baseline (n=5). (C) Representative flow cytometry analysis (left) and proportion (right) of activated B cells ($CD69^+$) isolated from colon lamina propria of WT and *Card9*$^{-/-}$ mice at baseline (n=5). Numbers in quadrants represent percent cells in each. Data expressed as mean ± SEM.

Supplementary figure S3 Area under the curve of bacterial count in feces of GF WT and GF *Card9*$^{-/-}$ mice infected with *C. rodentium*. Area under the curve (AUC) based in *C.*

rodentium count in feces of GF WT and GF *Card9*$^{-/-}$ mice (n=6) infected orally with 1 x 10^9 CFU of *C. rodentium.* Data expressed as mean ± SEM.

Supplementary figure S4 Rag2$^{-/-}$ and Rag2$^{-/-}$Card9$^{-/-}$ mice are equally susceptible to *C. rodentium* infection. WT, *Card9*$^{-/-}$, *Rag2*$^{-/-}$, and *Rag2*$^{-/-}$*Card9*$^{-/-}$ mice (n=5) were infected orally with 1 x 10^9 CFU of *C. rodentium*, and *C. rodentium* count in feces (up) and mouse survival (down) were determined. † denotes bacterial loads could not be determined beyond this time due to mouse lethality. Data expressed as mean ± SEM. **p < 0.01 by log rank test.

Supplementary figure S5 Experimental design of WT→GF and *Card9*$^{-/-}$→GF mice infection with *C. rodentium*. WT germ-free mice were inoculated with fecal suspension from the conventional wild-type (WT→GF) or *Card9*$^{-/-}$ (*Card9*$^{-/-}$→GF) mice. Three weeks after inoculation WT→GF and *Card9*$^{-/-}$→GF mice were infected by *C. rodentium*. The mice were sacrificed before (day 0) and 4, 12 and 22 days after infection.

Supplementary figure S6 Area under the curve of bacterial count in feces of WT→GF and *Card9*$^{-/-}$→GF mice infected with *C. rodentium*. Area under the curve (AUC) based in *C. rodentium* count in feces of WT→GF and *Card9*$^{-/-}$→GF mice (n=10) infected orally with 1 x 10^9 CFU of *C. rodentium.* Data expressed as mean ± SEM.

Supplementary figure S7 The microbiota of *Card9*$^{-/-}$ mice induces a dysregulated host transcriptomic response. (A and B) Microarray analysis of cecum tissue from WT→GF and *Card9*$^{-/-}$→GF mice (n=5) infected with *C. rodentium*. The Venn diagram represents the number of genes significantly downregulated (A) or upregulated (B) between day 0 and day 12 (Benjamini Hochberg $P < 0.05$). Histograms represent KEGG pathways.

Supplementary figure S8 Cecum expression in WT→GF and *Card9*$^{-/-}$→GF mice using microarray technology. Gene expression in cecum of WT→GF and *Card9*$^{-/-}$→GF mice was analyzed by principal component analysis before (day 0) and after (day 4, day 12 and day 22) infection with *C. rodentium*. The ellipses delimit WT→GF group (FWT in red) and *Card9*$^{-/-}$→GF group (FKO in black). The axes correspond to principal component 1 (x axis) and 2 (y axis).

Supplementary figure S9 *C. rodentium*-specific IgG quantification in feces of WT→GF and *Card9*$^{-/-}$→GF mice during *C. rodentium* infection. Concentration of *C. rodentium*-specific IgG in the feces of WT→GF and *Card9*$^{-/-}$→GF mice (n=10) infected with *C. rodentium*. Data expressed as mean ± SEM. *$p < 0.05$ by Mann-Whitney U test.

Supplementary figure S10 Bacterial taxa differentially enriched in WT→GF and *Card9*$^{-/-}$→GF mice before and during infection of *C. rodentium*. Differentially enriched bacterial phylotypes (using LEfSe pipeline) between WT→GF and *Card9*$^{-/-}$→GF mice (n=5) before and after *C. rodentium* infection. The heat map shows the relative abundance of OTUs.

Supplementary figure S11 Predicted bacterial metabolism differentially enriched in WT→GF and *Card9*$^{-/-}$→GF mice. Bacterial metabolism pathways differentially enriched in WT→GF and *Card9*$^{-/-}$→GF mice (n=5) before infection (inferred metagenomics using Picrust software).

Supplementary figure S12 Predicted sugar metabolism differentially enriched in WT and *Card9*$^{-/-}$ mice. Inferred metagenomics using Picrust software based on the bacterial 16S

rDNA gene sequence abundance in fecal content from WT and Card9$^{-/-}$ mice at baseline. The heat map shows the sugar metabolism differentially enriched in WT and Card9$^{-/-}$ mice before infection (D0).

Supplementary figure S13 MSs and PSs diet shape the microbiota in WT and *Card9*$^{-/-}$ mice. (A) Bacterial-taxon-based analysis at the phylum (left) and the family (right) level in the feces from WT and *Card9*$^{-/-}$ mice (n=7) before infection. Mice were fed either a monosaccharides (MSs) or a polysaccharides (PSs) diet during 1 week. (B) Differences in abundance are shown for the bacterial taxa in WT and *Card9*$^{-/-}$ mice (n=7) fed with MSs or PSs diet (generated using LEfSe pipeline).

SUPPLEMENTAL REFERENCES

1 Barthel M, Hapfelmeier S, Quintanilla-Martínez L, *et al.* Pretreatment of mice with streptomycin provides a Salmonella enterica serovar Typhimurium colitis model that allows analysis of both pathogen and host. *Infect Immun* 2003;71:2839–58.
2 Tap J, Furet J-PP, Bensaada M, *et al.* Gut microbiota richness promotes its stability upon increased dietary fibre intake in healthy adults. *Environ Microbiol* 2016;17:4954–64.
3 Tomas J, Wrzosek L, Bouznad N, *et al.* Primocolonization is associated with colonic epithelial maturation during conventionalization. *FASEB J* 2013;27:645–55.
4 Sokol H, Conway KL, Zhang M, *et al.* Card9 mediates intestinal epithelial cell restitution, T-helper 17 responses, and control of bacterial infection in mice. *Gastroenterology* 2013;145:591–601.
5 Lamas B, Richard ML, Leducq V, *et al.* CARD9 impacts colitis by altering gut microbiota metabolism of tryptophan into aryl hydrocarbon receptor ligands. *Nat Med* 2016;22:598–605.
6 Schmieder R, Edwards R. Quality control and preprocessing of metagenomic datasets. *Bioinformatics* 2011;27:863–4.
7 Magoč T, Salzberg SL. FLASH: fast length adjustment of short reads to improve genome assemblies. *Bioinformatics* 2011;27:2957–63.
8 Caporaso JG, Kuczynski J, Stombaugh J, *et al.* QIIME allows analysis of high-throughput community sequencing data. *Nat Methods* 2010;7:335–6.
9 Edgar RC. Search and clustering orders of magnitude faster than BLAST. *Bioinformatics* 2010;26:2460–1.
10 McDonald D, Price MN, Goodrich J, *et al.* An improved Greengenes taxonomy with explicit ranks for ecological and evolutionary analyses of bacteria and archaea. *ISME J* 2012;6:610–8.
11 Bolstad BM, Irizarry RA, Astrand M, *et al.* A comparison of normalization methods

for high density oligonucleotide array data based on variance and bias. *Bioinformatics* 2003;19:185–93.
12 Smyth GK. Linear models and empirical bayes methods for assessing differential expression in microarray experiments. *Stat Appl Genet Molecular Biol* 2004;3:Article3.
13 Huang DW a W, Sherman BT, Lempicki RA. Systematic and integrative analysis of large gene lists using DAVID bioinformatics resources. *Nat Protoc* 2009;4:44–57.
14 Huang DW a W, Sherman BT, Lempicki RA. Bioinformatics enrichment tools: paths toward the comprehensive functional analysis of large gene lists. *Nucleic acids Res* 2009;37:1–13.

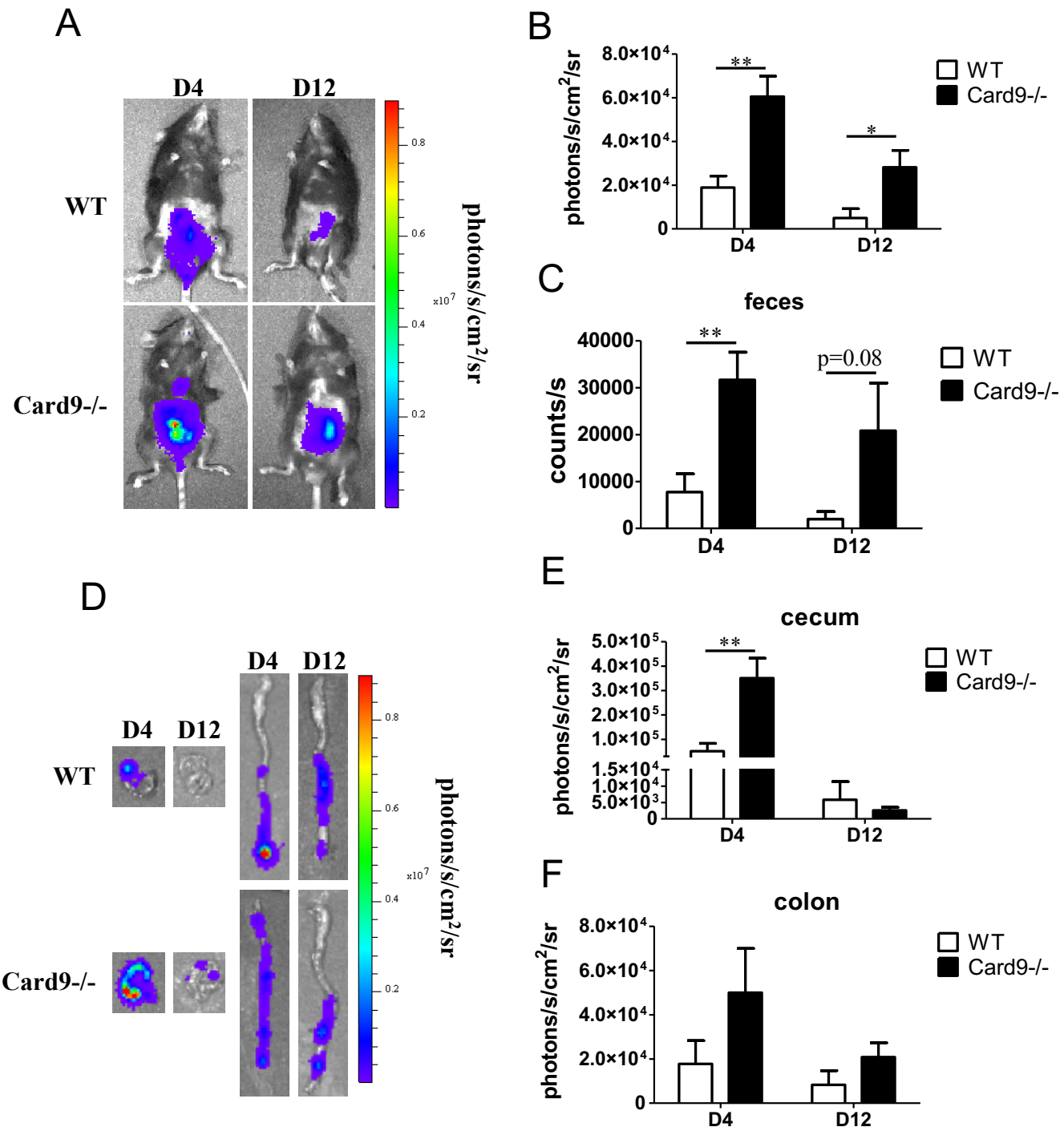
A
D4
D12
WT
Card9-/-
photons/s/cm2/sr
B
photons/s/cm2/sr
8.0×10^4
6.0×10^4
4.0×10^4
2.0×10^4
0
**
*
D4
D12
WT
Card9-/-
C
feces
counts/s
40000
30000
20000
10000
0
**
p=0.08
D4
D12
WT
Card9-/-
D
D4
D12
WT
Card9-/-
photons/s/cm2/sr
E
cecum
photons/s/cm2/sr
5.0×10^5
4.0×10^5
3.0×10^5
2.0×10^5
1.0×10^5
1.5×10^4
1.0×10^4
5.0×10^3
0
**
D4
D12
WT
Card9-/-
F
colon
photons/s/cm2/sr
8.0×10^4
6.0×10^4
4.0×10^4
2.0×10^4
0
D4
D12
WT
Card9-/-

A

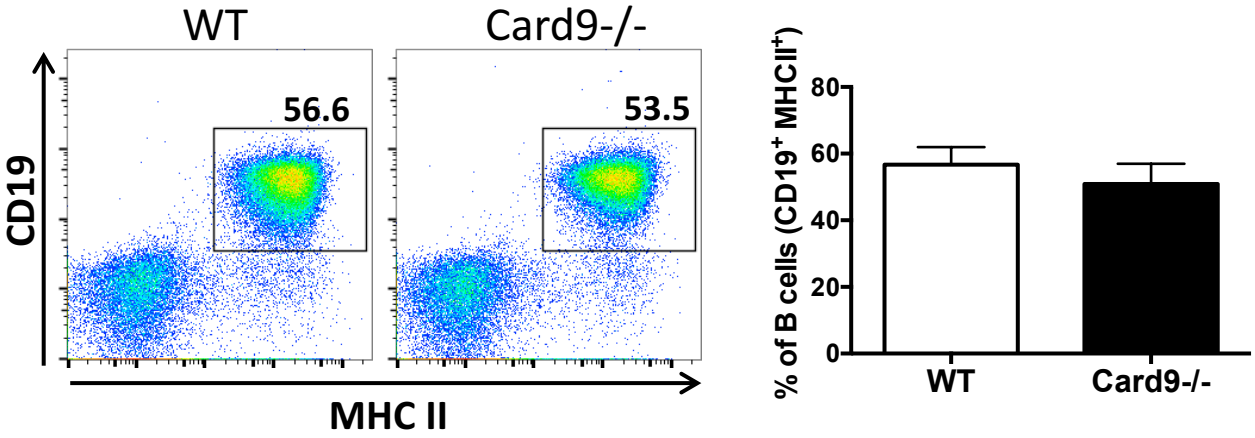
WT
Card9-/-
56.6
53.5
CD19
MHC II
% of B cells (CD19+ MHCII+)
80
60
40
20
0
WT
Card9-/-

B

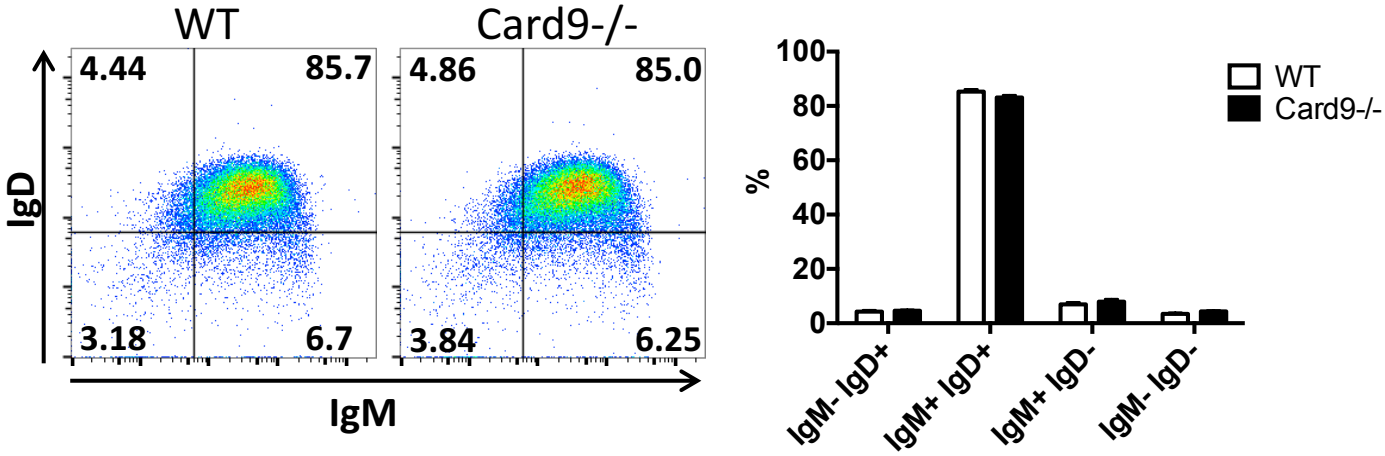
WT
Card9-/-
4.44
85.7
3.18
6.7
4.86
85.0
3.84
6.25
IgD
IgM
%
100
80
60
40
20
0
WT
Card9-/-
IgM- IgD+
IgM+ IgD+
IgM+ IgD-
IgM- IgD-

C

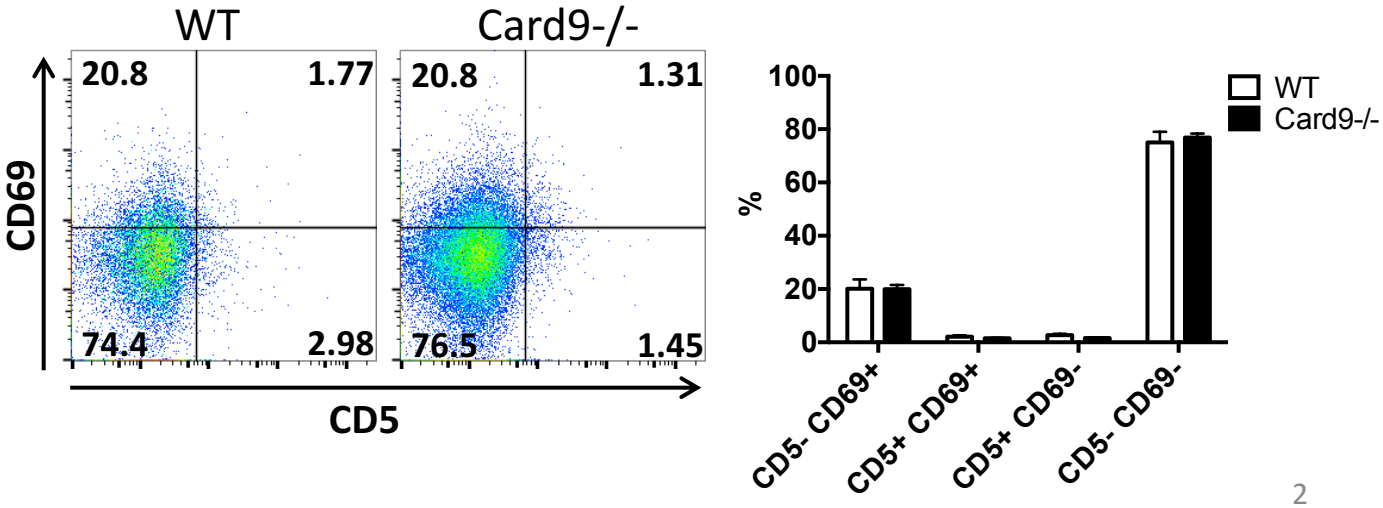
WT
Card9-/-
20.8
1.77
74.4
2.98
20.8
1.31
76.5
1.45
CD69
CD5
%
100
80
60
40
20
0
WT
Card9-/-
CD5- CD69+
CD5+ CD69+
CD5+ CD69-
CD5- CD69-

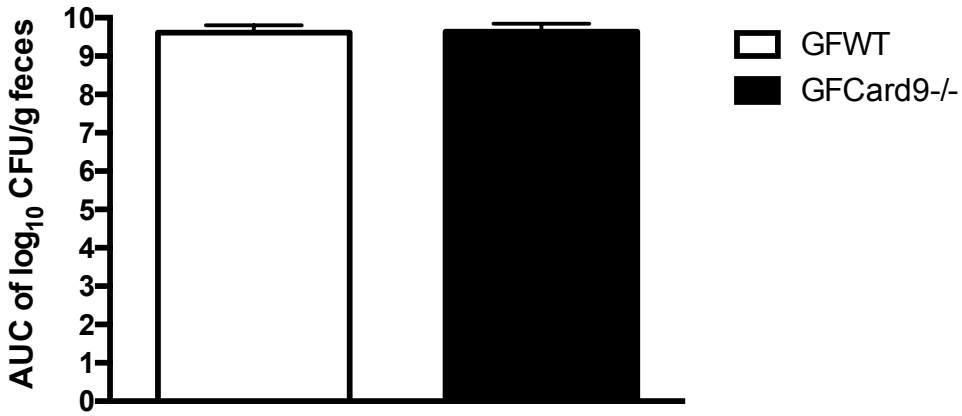
AUC of log10 CFU/g feces
10
9
8
7
6
5
4
3
2
1
0
GFWT
GFCard9-/-

Supp Figure S4

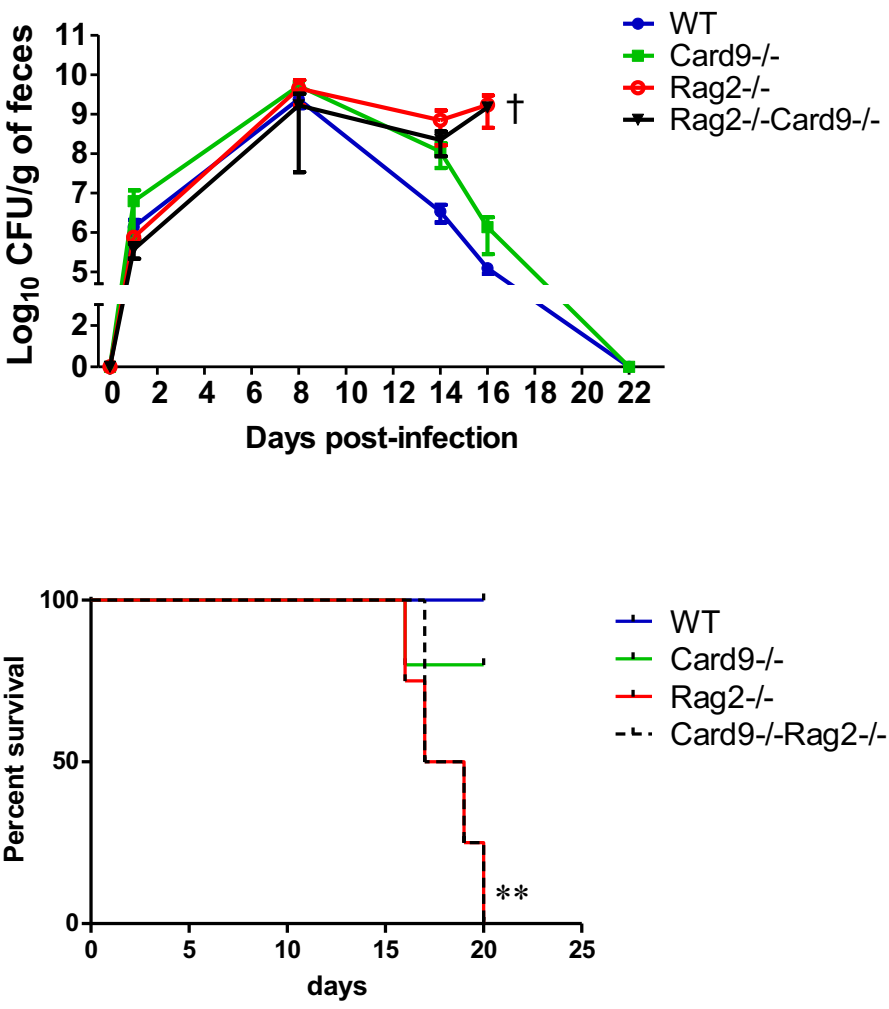

Supp Figure S5

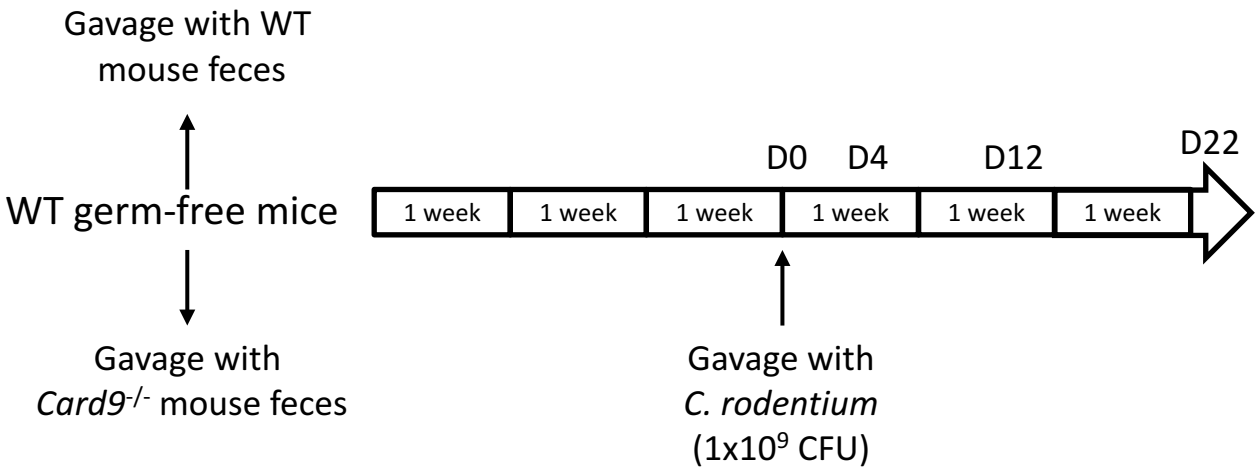

Supp Figure S6

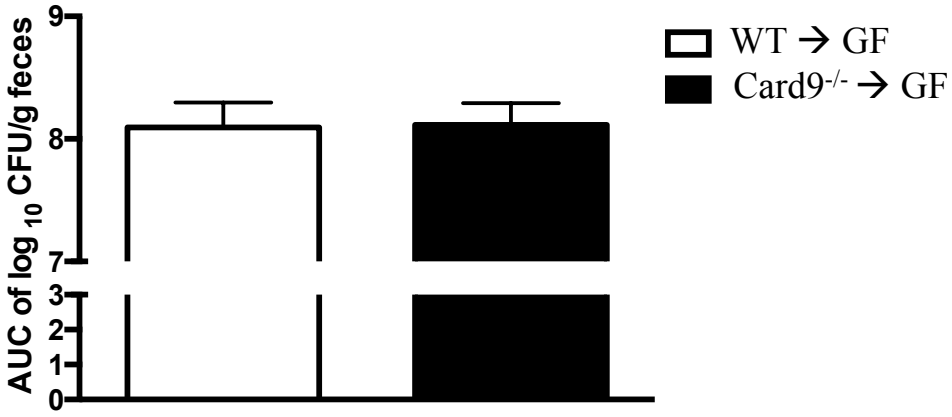

Supp Figure S7

A

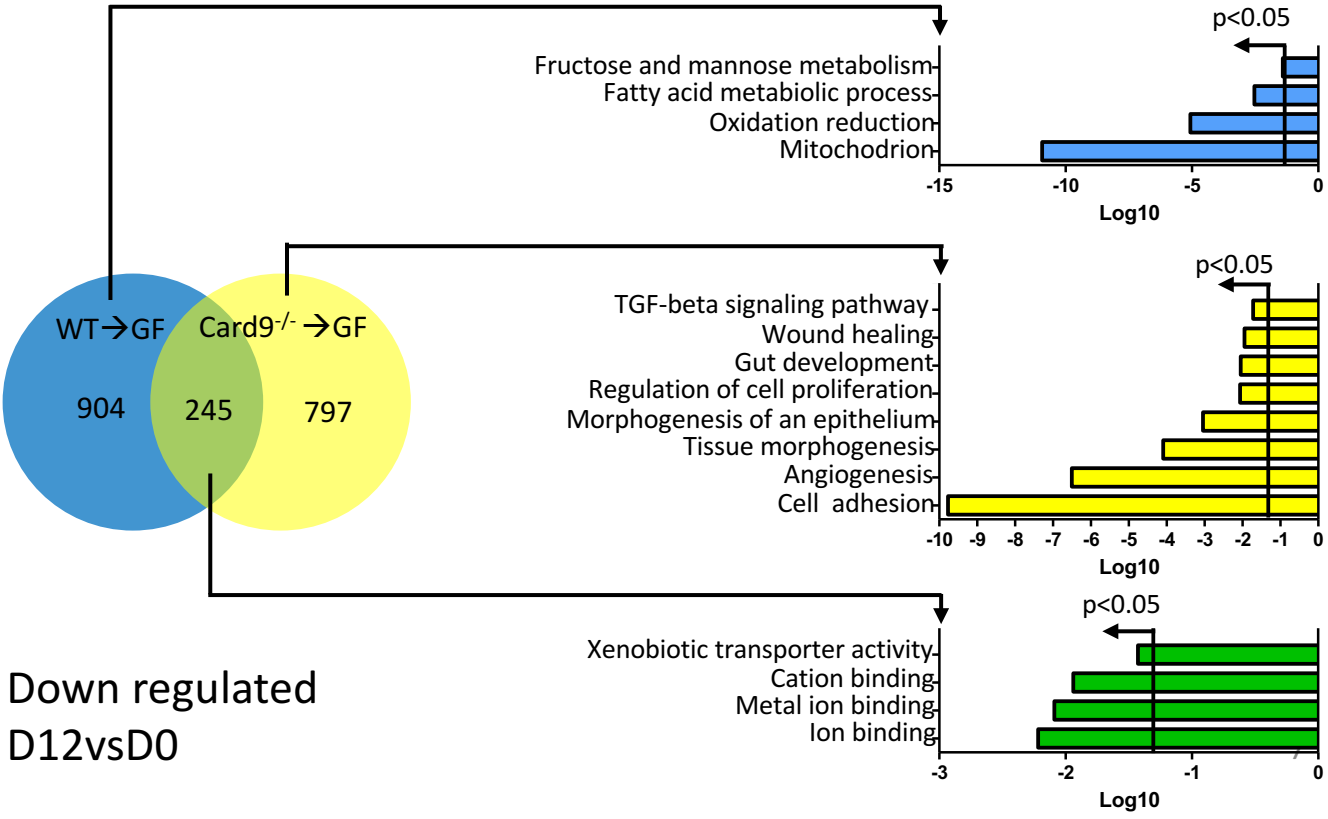

Down regulated
D12vsD0

B

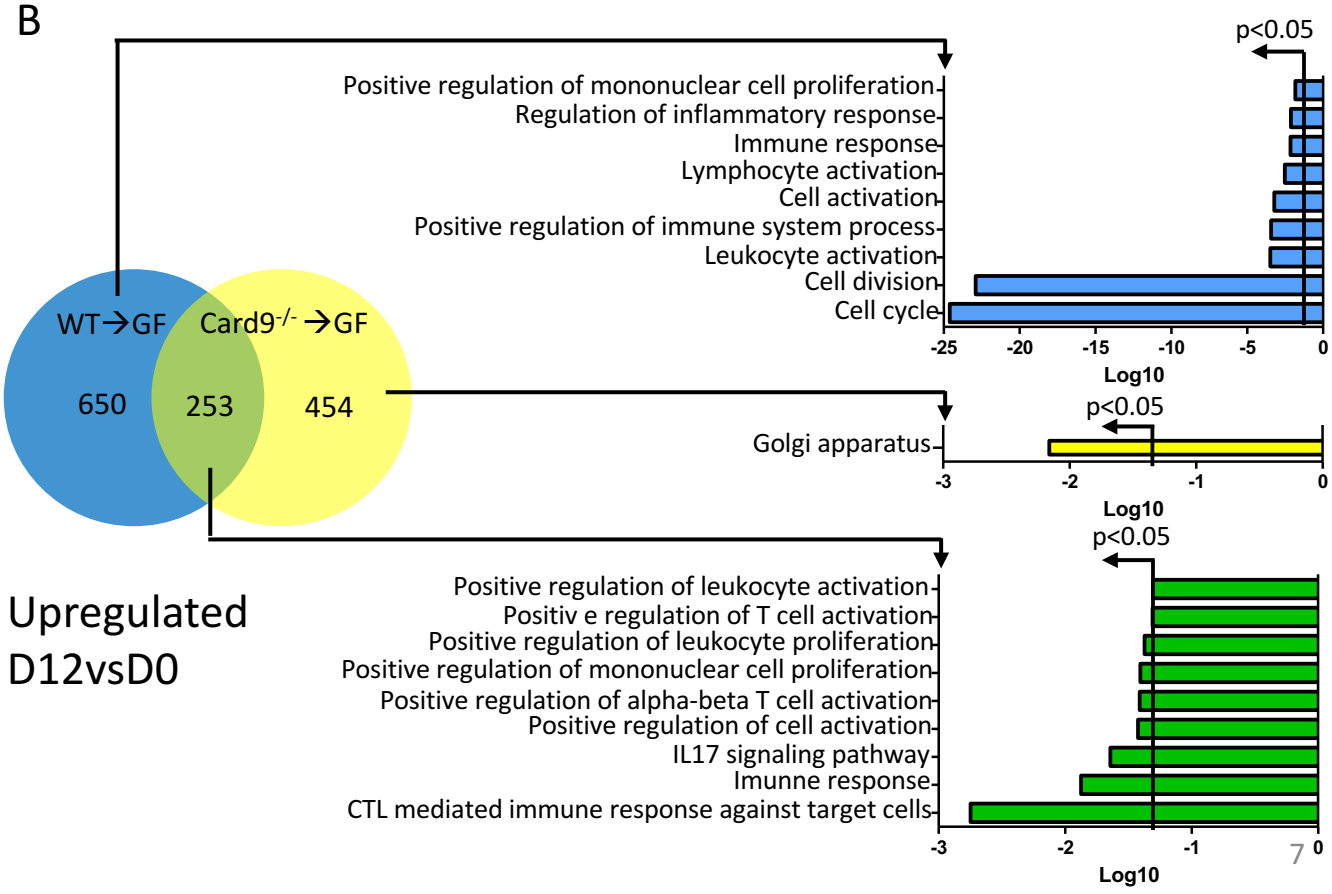

Upregulated
D12vsD0

D0

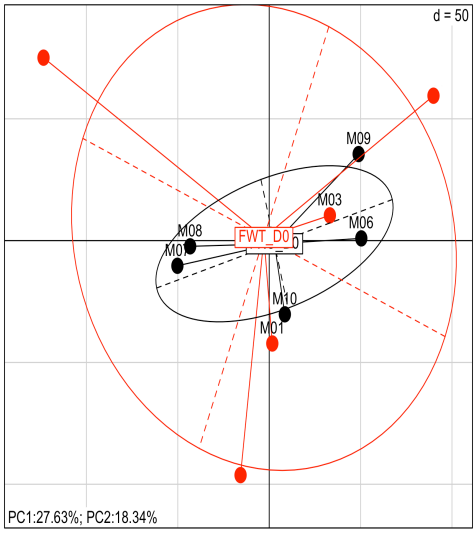
d = 50
M09
M03
M08
FWT_D0
M06
M01
M10
M01
PC1:27.63%; PC2:18.34%

D4

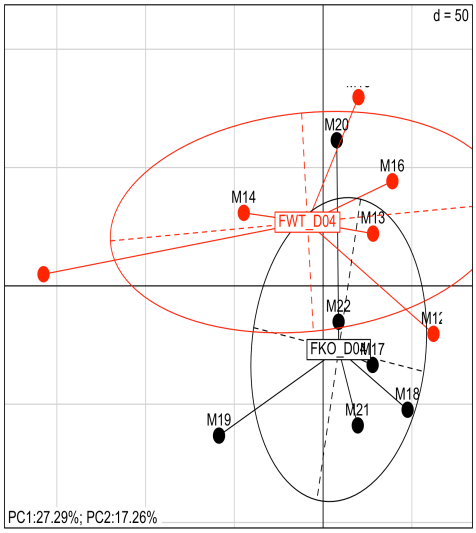
d = 50
M20
M16
M14
FWT_D04
M13
M22
FKO_D04
M17
M18
M19
M21
PC1:27.29%; PC2:17.26%

D12

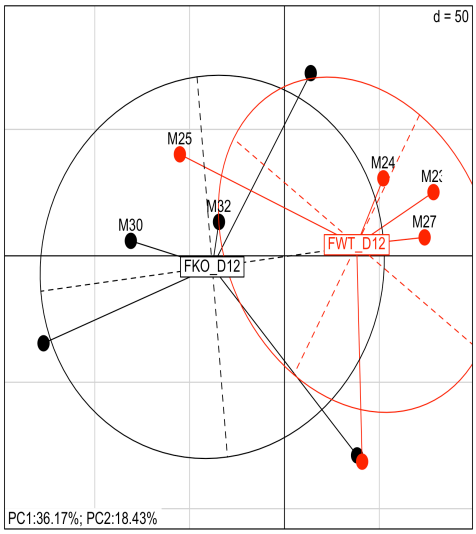
d = 50
M25
M24
M30
M32
M27
FWT_D12
FKO_D12
PC1:36.17%; PC2:18.43%

D22

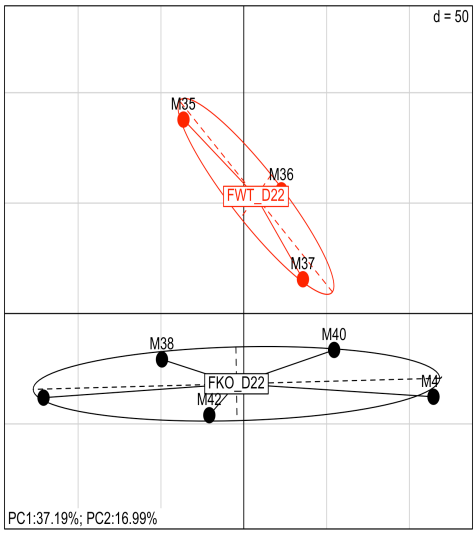
d = 50
M35
M36
FWT_D22
M37
M38
M40
FKO_D22
M42
PC1:37.19%; PC2:16.99%

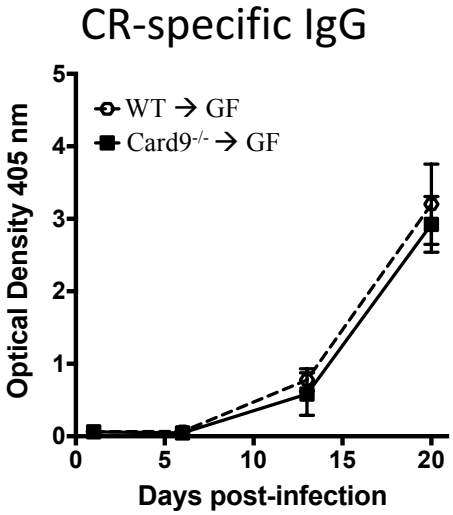
CR-specific IgG
WT → GF
Card9-/- → GF
Optical Density 405 nm
0
1
2
3
4
5
0
5
10
15
20
Days post-infection

Supp Figure S10

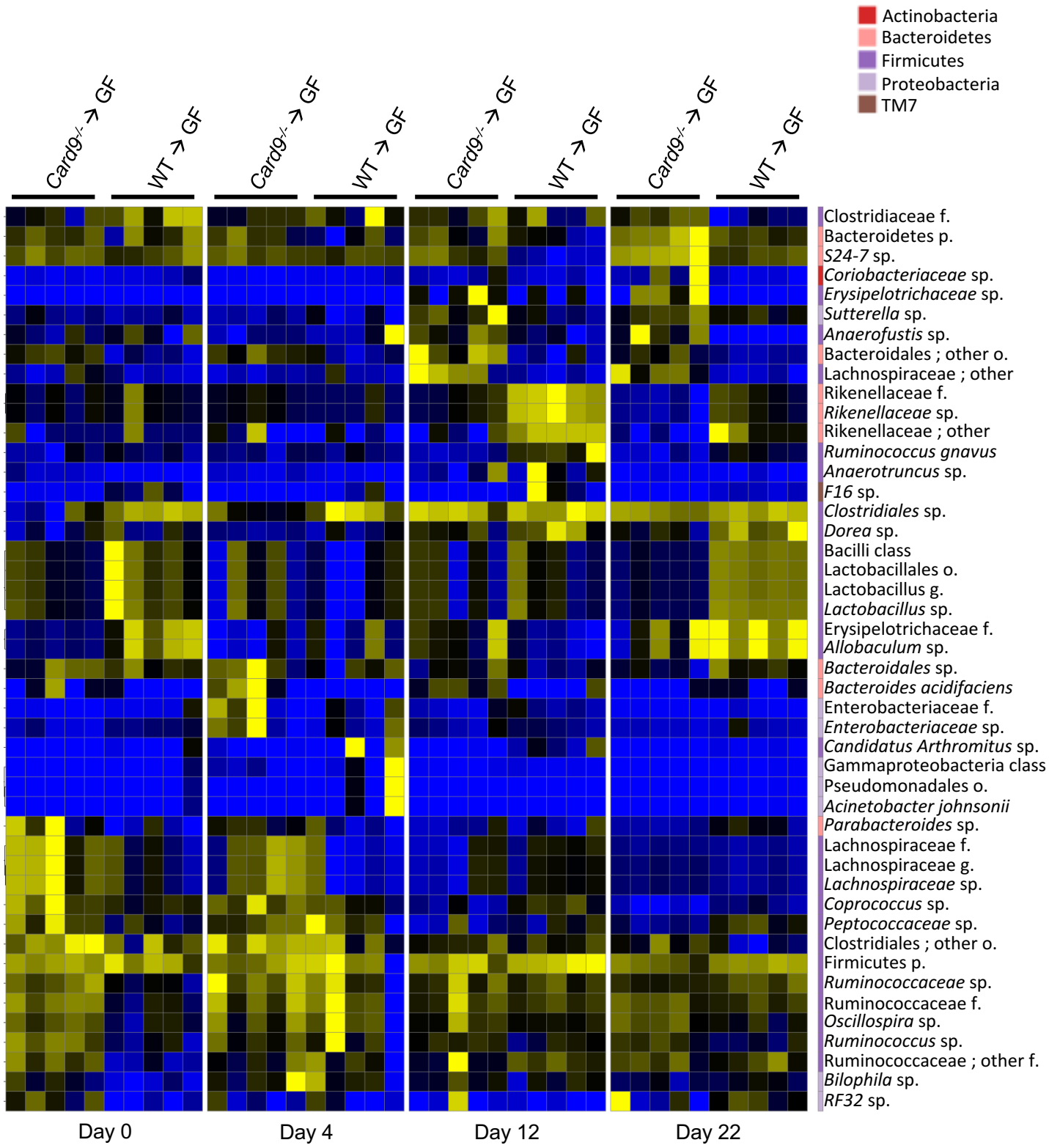

Supp Figure S11

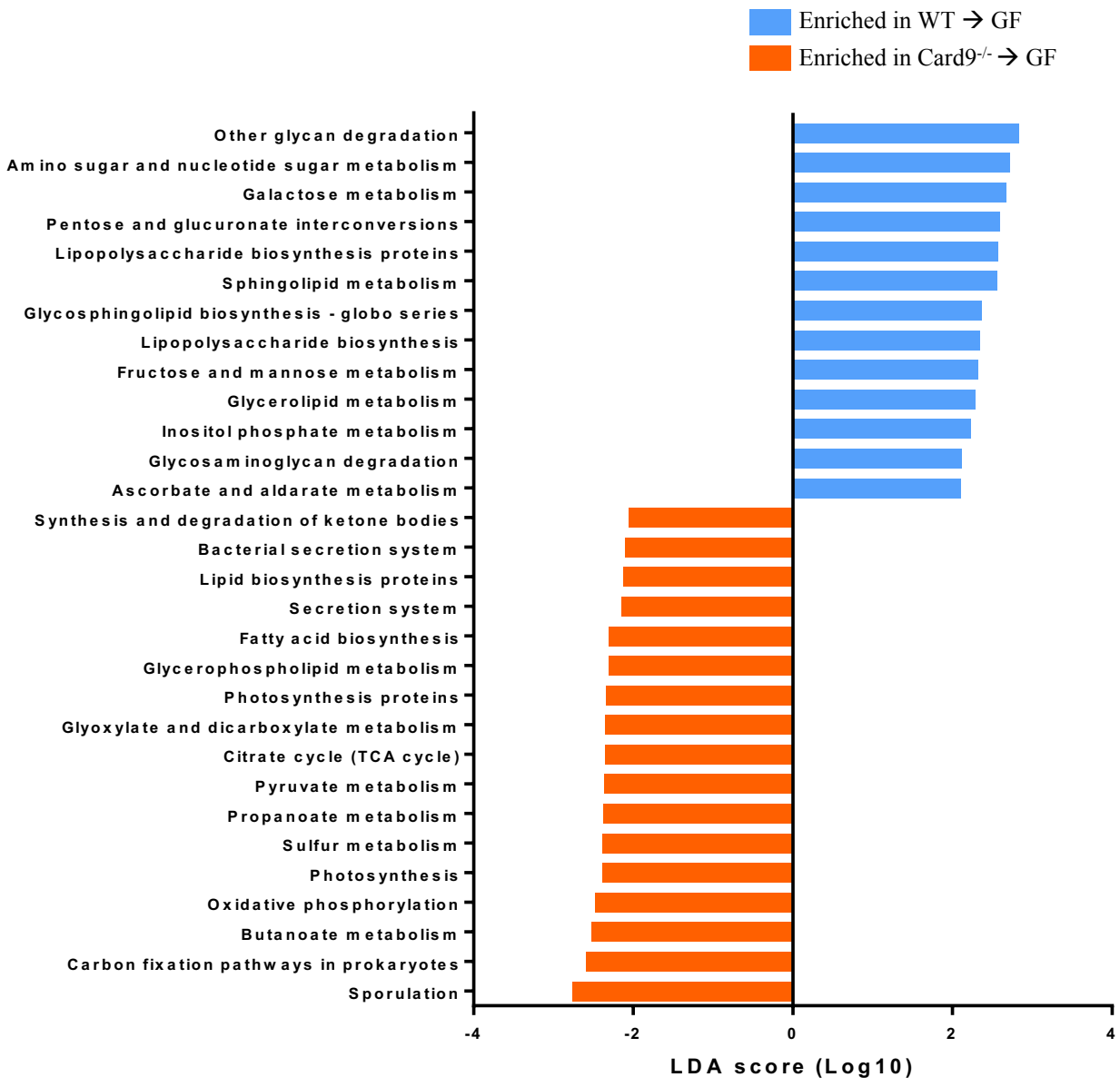

Supp Figure S12

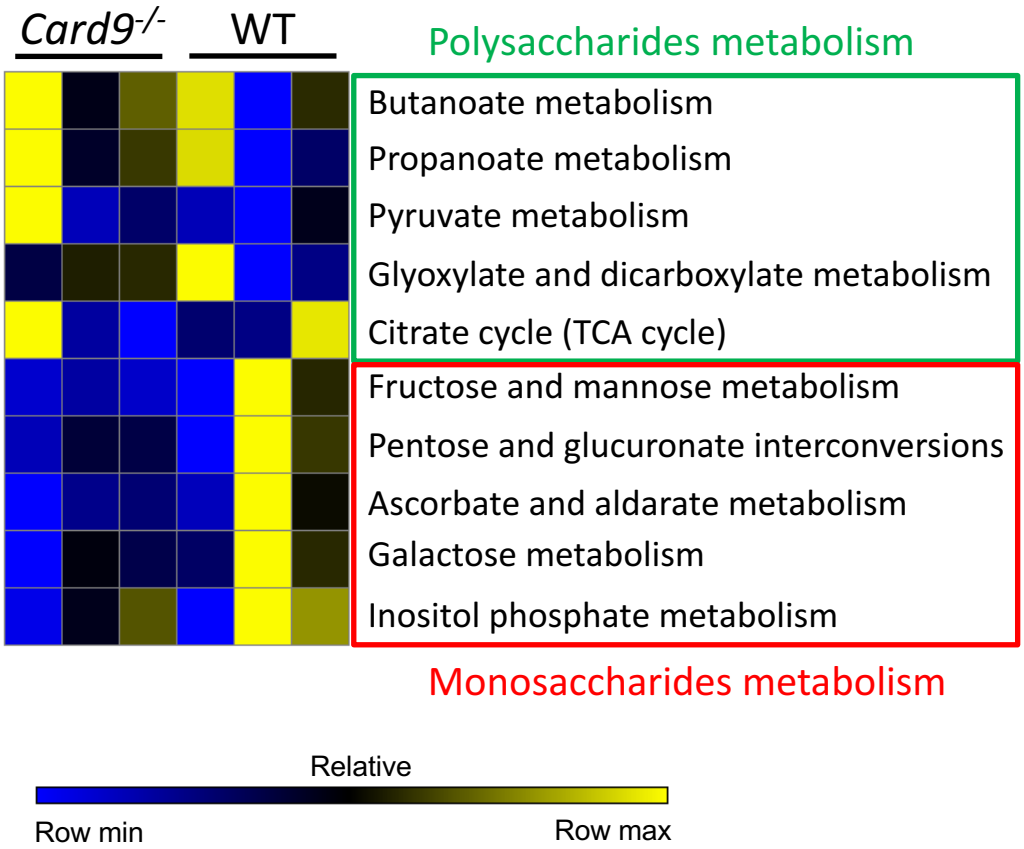

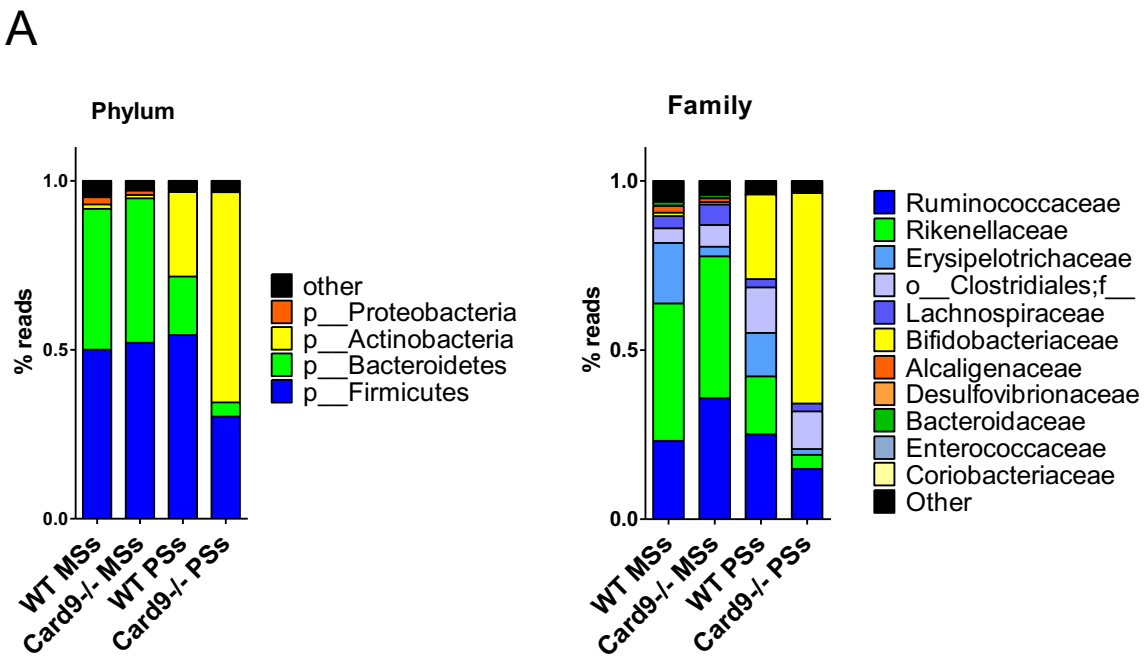
A
Phylum
% reads
1.0
0.5
0.0
WT MSs
Card9-/- MSs
WT PSs
Card9-/- PSs
other
p__Proteobacteria
p__Actinobacteria
p__Bacteroidetes
p__Firmicutes
Family
% reads
1.0
0.5
0.0
WT MSs
Card9-/- MSs
WT PSs
Card9-/- PSs
Ruminococcaceae
Rikenellaceae
Erysipelotrichaceae
o__Clostridiales;f__
Lachnospiraceae
Bifidobacteriaceae
Alcaligenaceae
Desulfovibrionaceae
Bacteroidaceae
Enterococcaceae
Coriobacteriaceae
Other

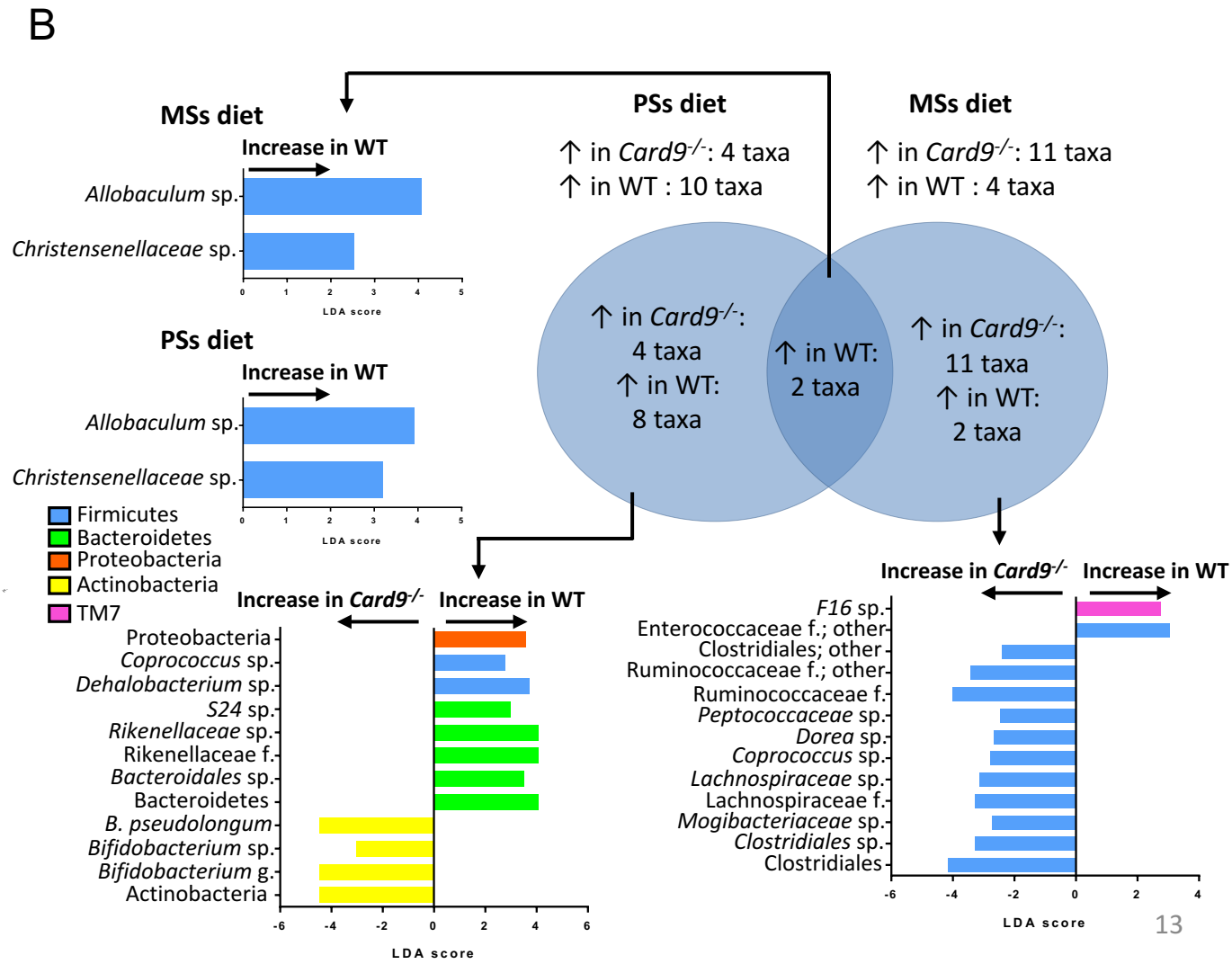
B
MSs diet
Increase in WT
Allobaculum sp.
Christensenellaceae sp.
LDA score
PSs diet
Increase in WT
Allobaculum sp.
Christensenellaceae sp.
LDA score
Firmicutes
Bacteroidetes
Proteobacteria
Actinobacteria
TM7
PSs diet
↑ in Card9-/-: 4 taxa
↑ in WT : 10 taxa
MSs diet
↑ in Card9-/-: 11 taxa
↑ in WT : 4 taxa
↑ in Card9-/-: 4 taxa
↑ in WT: 8 taxa
↑ in WT: 2 taxa
↑ in Card9-/-: 11 taxa
↑ in WT: 2 taxa
Increase in Card9-/-
Increase in WT
Proteobacteria
Coprococcus sp.
Dehalobacterium sp.
S24 sp.
Rikenellaceae sp.
Rikenellaceae f.
Bacteroidales sp.
Bacteroidetes
B. pseudolongum
Bifidobacterium sp.
Bifidobacterium g.
Actinobacteria
LDA score
Increase in Card9-/-
Increase in WT
F16 sp.
Enterococcaceae f.; other
Clostridiales; other
Ruminococcaceae f.; other
Ruminococcaceae f.
Peptococcaceae sp.
Dorea sp.
Coprococcus sp.
Lachnospiraceae sp.
Lachnospiraceae f.
Mogibacteriaceae sp.
Clostridiales sp.
Clostridiales
LDA score